The Underlying Event: Z-boson vs Dijet

Rick Field, Henry Frisch, Richard Haas, and David Stuart

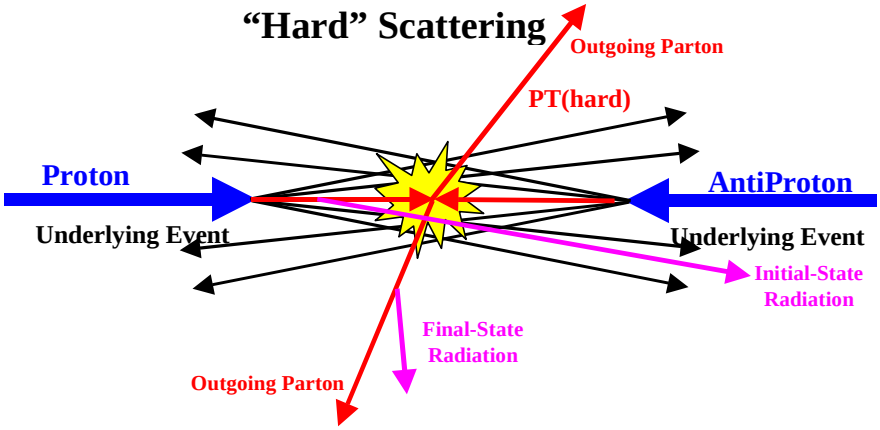

Fig. 1. Illustration of a proton-antiproton collision in which a "hard" 2-to-2 parton scattering with transverse momentum, $P_T(\text{hard})$, has occurred. The resulting "dijet" event contains particles that originate from the two outgoing partons (plus final-state radiation) and particles that come from the breakup of the proton and antiproton (*i.e.* "beam-beam remnants"). The "underlying event" consists of the beam-beam remnants plus initial-state radiation.

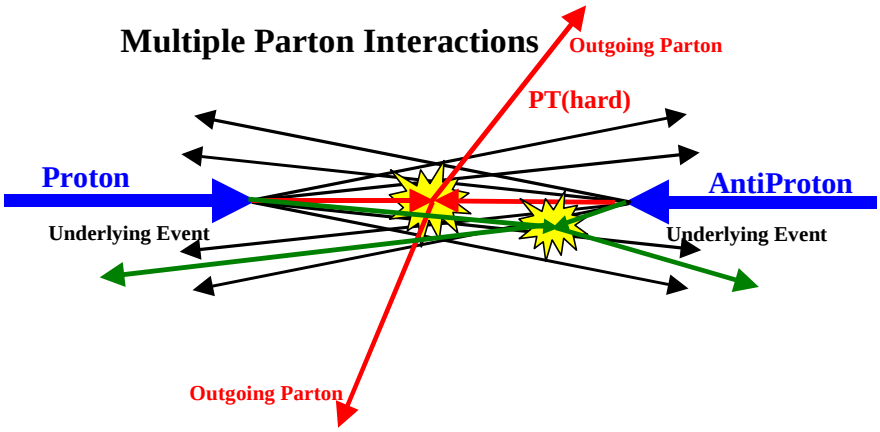

Fig. 2. Illustration of a proton-antiproton collision in which a multiple parton interaction has occurred. In addition to the "hard" 2-to-2 parton scattering with transverse momentum, $P_T(\text{hard})$, there is an additional "semi-hard" parton-parton scattering that contributes particles to the "underlying event". For PYTHIA, we include the contributions from multiple parton scattering in the beam-beam remnant component.

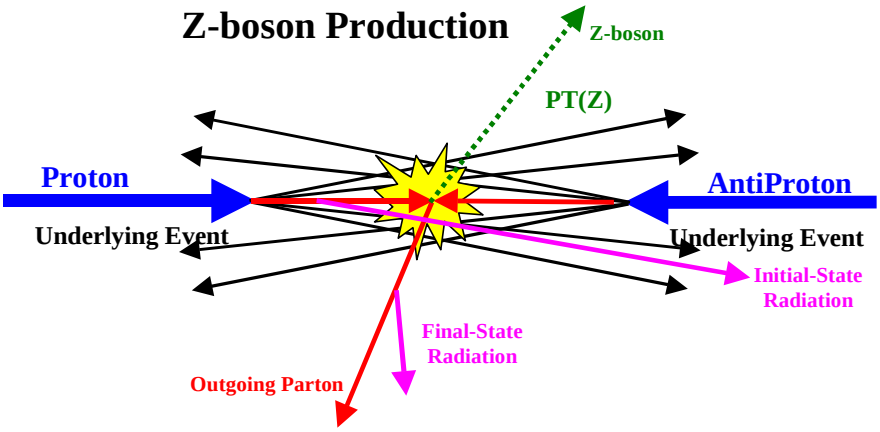

Fig. 3. Illustration of a proton-antiproton collision in which a Z-boson with large transverse momentum, $P_T(Z)$, has been produced. The resulting event contains particles that originate from the "away-side" outgoing parton (plus final-state radiation) and particles that come from the breakup of the proton and antiproton (*i.e.* "beam-beam remnants"). The "underlying event" consists of the beam-beam remnants plus initial-state radiation.

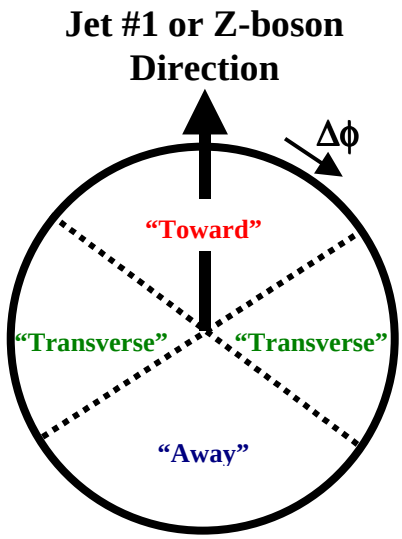

Fig. 4. Illustration of correlations in azimuthal angle $\Delta\phi$ relative to the direction of the leading charged jet in the event, jet#1, or the Z-boson. The angle $\Delta\phi = |\phi - \phi_{jet\#1}|$ is the relative azimuthal angle between charged particles and the direction of jet#1 or the Z-boson. The region $|\Delta\phi| < 60^o$ is referred to as "toward" (*includes particles in jet#1 but does not include the decay products of the Z-boson*) and the region $|\Delta\phi| > 120^o$ is called "away". The "transverse" region is defined by $60^o < |\Delta\phi| < 120^o$. Each region, "toward", "transverse", and "away" covers the same range $|\Delta\eta| \times |\Delta\phi| = 2 \times 120^o$.

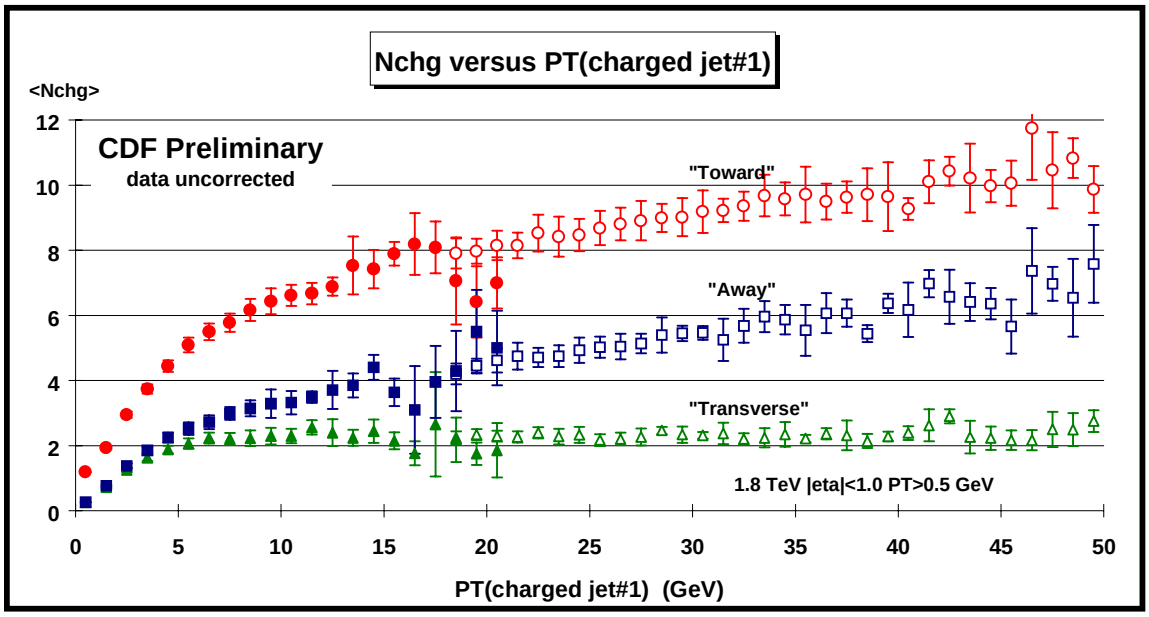

Fig. 5. The average number of "toward" ($|\Delta\phi|<60^{O}$), "transverse" ($60<|\Delta\phi|<120^{O}$), and "away" ($|\Delta\phi|>120^{O}$) charged particles ($P_T > 0.5$ GeV, $|\eta| < 1$, including jet#1) as a function of the transverse momentum of the leading charged particle jet. Each point corresponds to the <Nchg> in a 1 GeV bin. The solid (open) points are the Min-Bias (JET20) data. The errors on the (*uncorrected*) data include both statistical and correlated systematic uncertainties. The "toward", "transverse", and "away" regions are defined in Fig. 4.

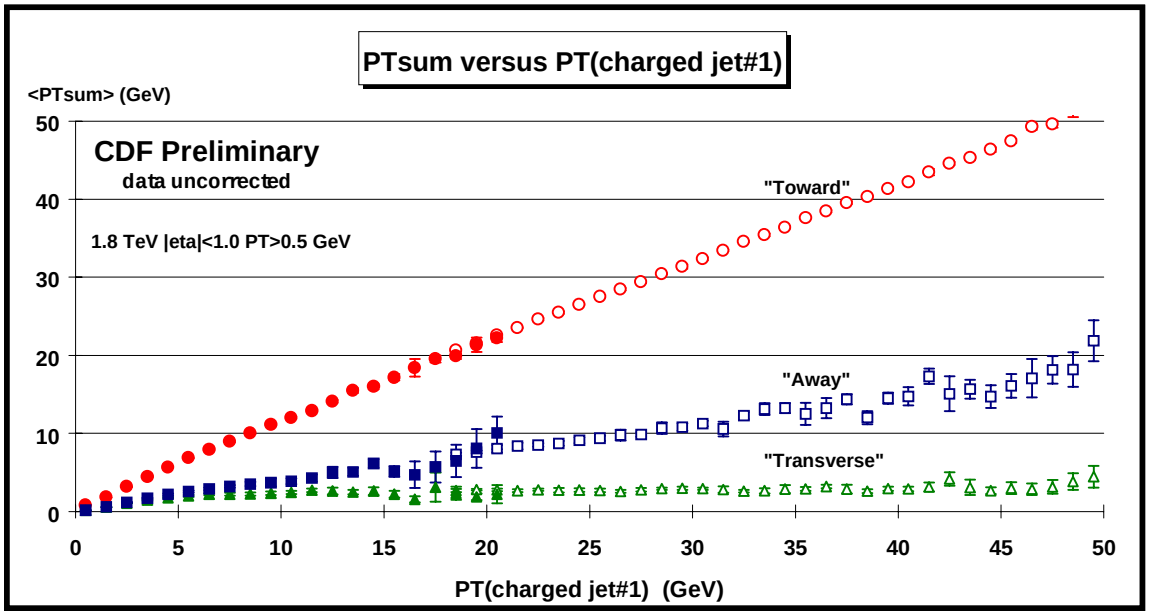

Fig. 6. The average *scalar* P_T sum of "toward" ($|\Delta\phi|<60^{O}$), "transverse" ($60<|\Delta\phi|<120^{O}$), and "away" ($|\Delta\phi|>120^{O}$) charged particles ($P_T > 0.5$ GeV, $|\eta| < 1$, including jet#1) as a function of the transverse momentum of the leading charged particle jet. Each point corresponds to the <PTsum> in a 1 GeV bin. The solid (open) points are the Min-Bias (JET20) data. The errors on the (*uncorrected*) data include both statistical and correlated systematic uncertainties. The "toward", "transverse", and "away" regions are defined in Fig. 4.

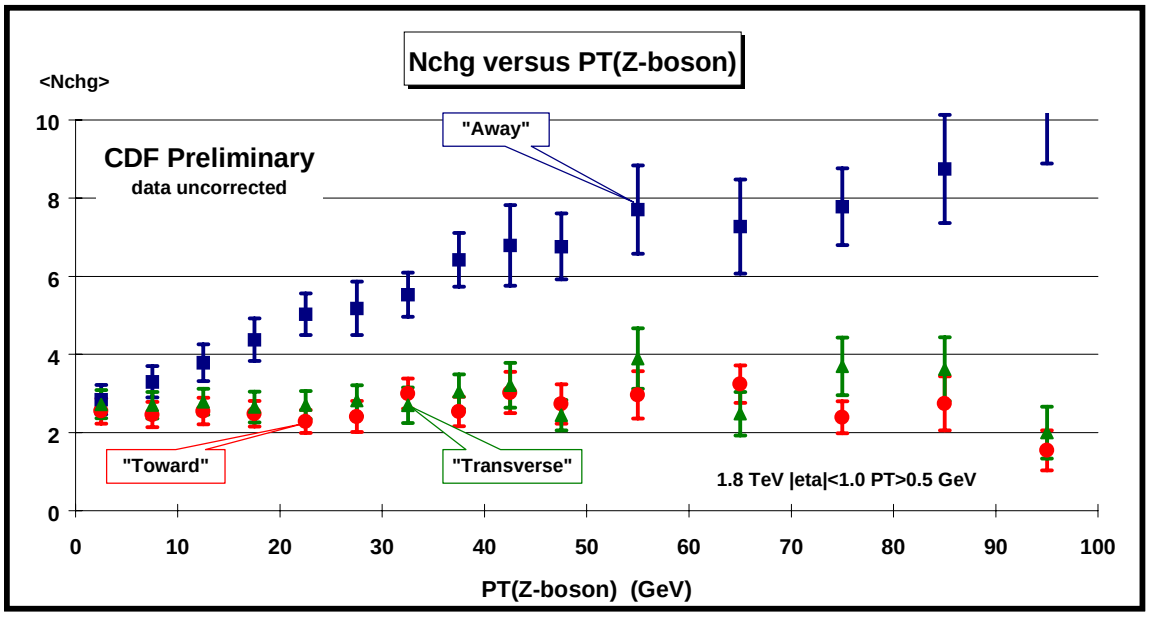

Fig. 7. The average number of "toward" ($|\Delta\phi|<60^{O}$), "transverse" ($60<|\Delta\phi|<120^{O}$), and "away" ($|\Delta\phi|>120^{O}$) charged particles ($P_T > 0.5$ GeV, $|\eta| < 1$, excluding decay products of the Z-boson) as a function of the transverse momentum of the Z-boson. The errors on the (*uncorrected*) data include both statistical and correlated systematic uncertainties. The "toward", "transverse", and "away" regions are defined in Fig. 4.

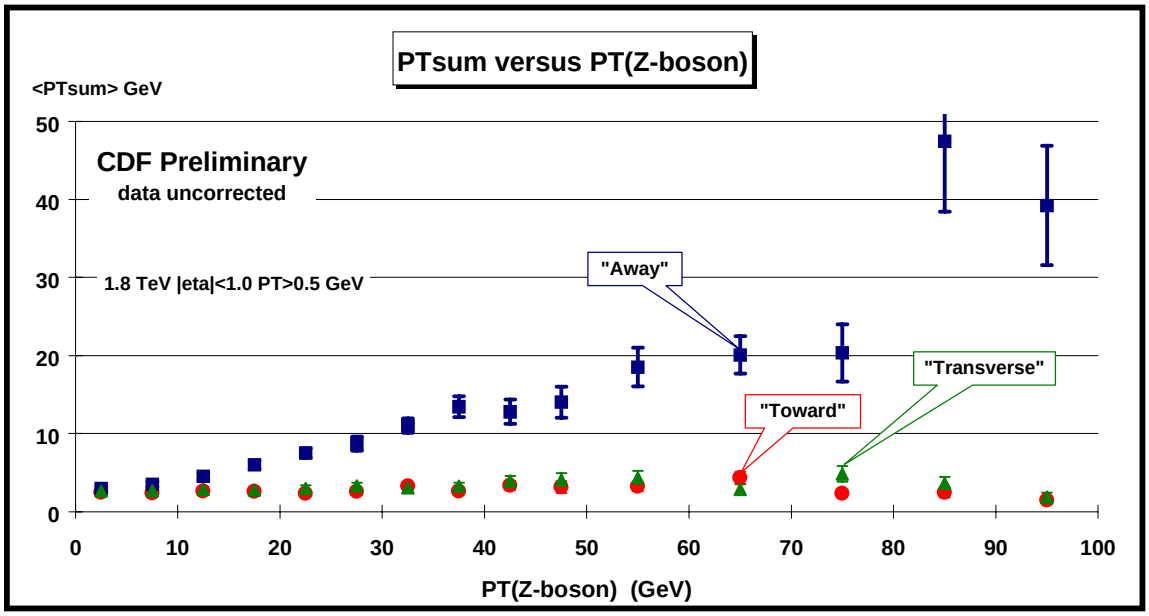

Fig. 8. The average *scalar* P_T sum of "toward" ($|\Delta\phi|<60^{O}$), "transverse" ($60<|\Delta\phi|<120^{O}$), and "away" ($|\Delta\phi|>120^{O}$) charged particles ($P_T > 0.5$ GeV, $|\eta| < 1$, exculding the decay products of the Z-boson) as a function of the transverse momentum of the Z-boson. The errors on the (*uncorrected*) data include both statistical and correlated systematic uncertainties. The "toward", "transverse", and "away" regions are defined in Fig. 4.

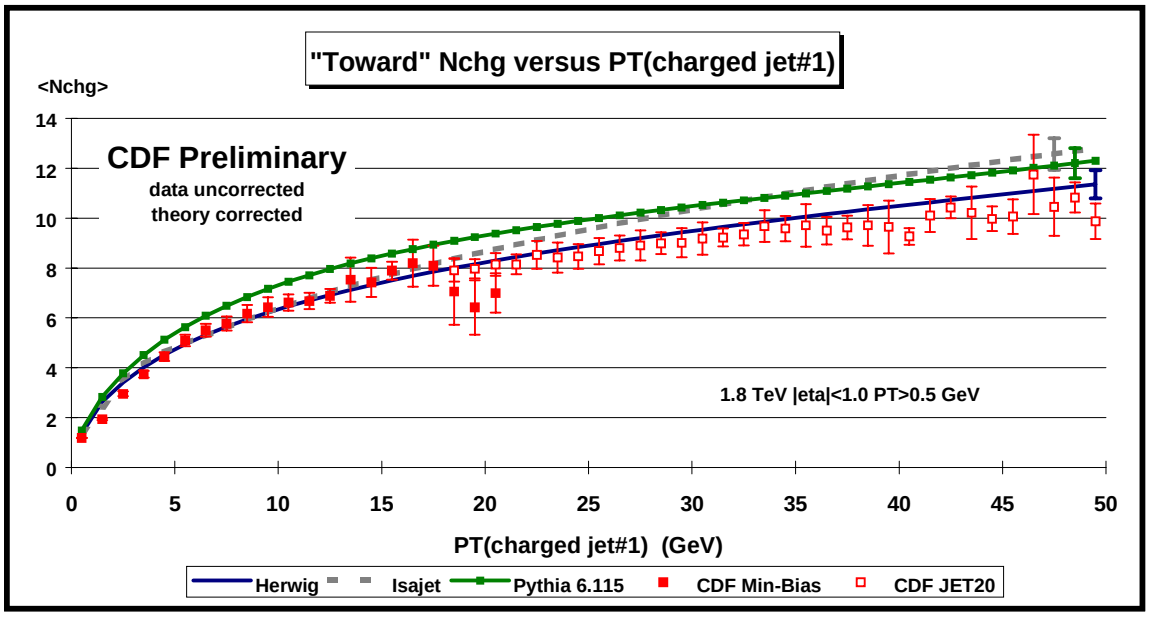

Fig. 9. Dijet data from Fig. 5 on the average number of charged particles (P_T > 0.5 GeV and |η| < 1) as a function of P_T (jet#1) (*leading charged jet*) for the "toward" region defined in Fig. X compared with the QCD "hard scattering" Monte-Carlo predictions of HERWIG 5.9, ISAJET 7.32, and PYTHIA 6.115. Each point corresponds to the "toward" <Nchg> in a 1 GeV bin. The errors on the (*uncorrected*) data include both statistical and correlated systematic uncertainties. The theory curves are corrected for the track finding efficiency and have an error (*statistical plus systematic*) of around 5%.

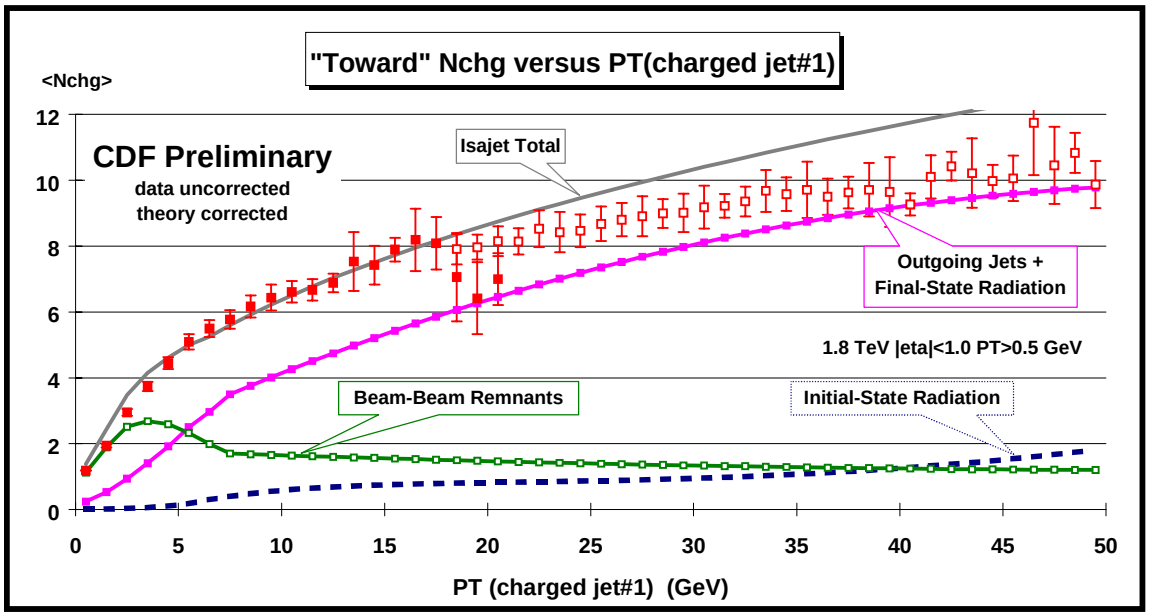

Fig. 10. Dijet data from Fig. 5 on the average number of charged particles (P_T > 0.5 GeV and |η| < 1) as a function of PT(jet#1) (*leading charged jet*) for the "toward" region defined in Fig. X compared with the QCD "hard scattering" Monte-Carlo predictions of ISAJET 7.32. The predictions of ISAJET are divided into three categories: charged particles that arise from the break-up of the beam and target (*beam-beam remnants*), charged particles that arise from initial-state radiation, and charged particles that result from the outgoing jets plus final-state radiation (see Fig. 1). The errors on the (*uncorrected*) data include both statistical and correlated systematic uncertainties. The theory curves are corrected for the track finding efficiency and have an error (*statistical plus systematic*) of around 5%.

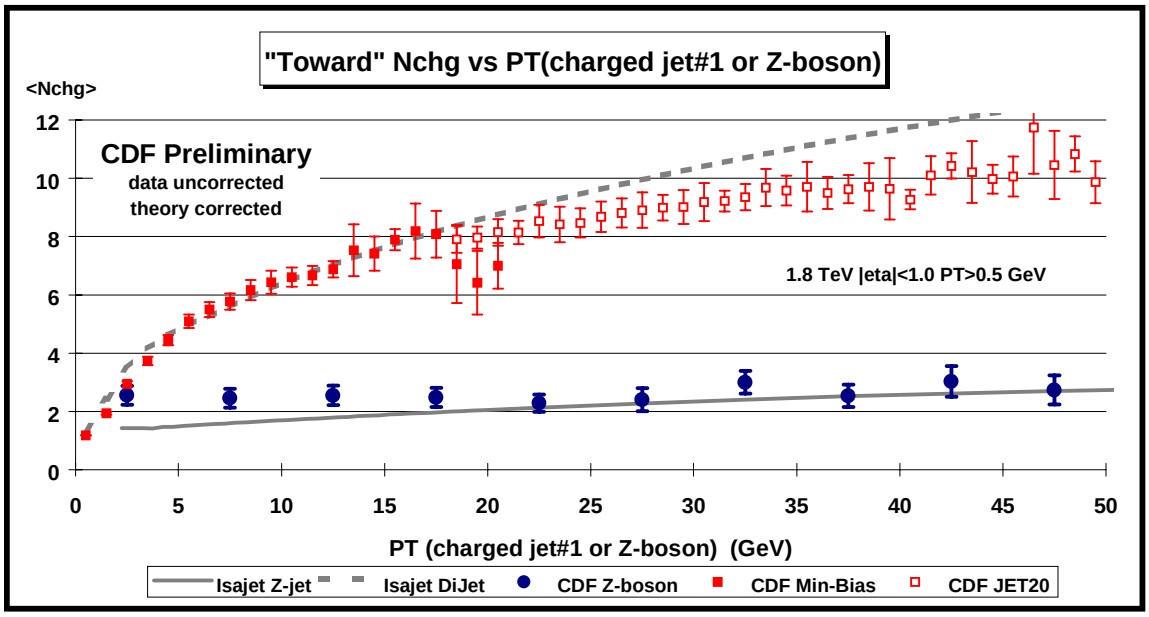

Fig. 11. Comparison of the dijet data from Fig. 5 and the Z-boson data from Fig. 7 on the average number of charged particles ($P_T > 0.5$ GeV and $|\eta| < 1$) for the "toward" region defined in Fig. 4. The plot shows the QCD Monte-Carlo predictions of ISAJET 7.32 for dijet (dashed) and "Z-jet" (solid) production. The errors on the (*uncorrected*) data include both statistical and correlated systematic uncertainties. The theory curves are corrected for the track finding efficiency and have an error (*statistical plus systematic*) of around 5%.

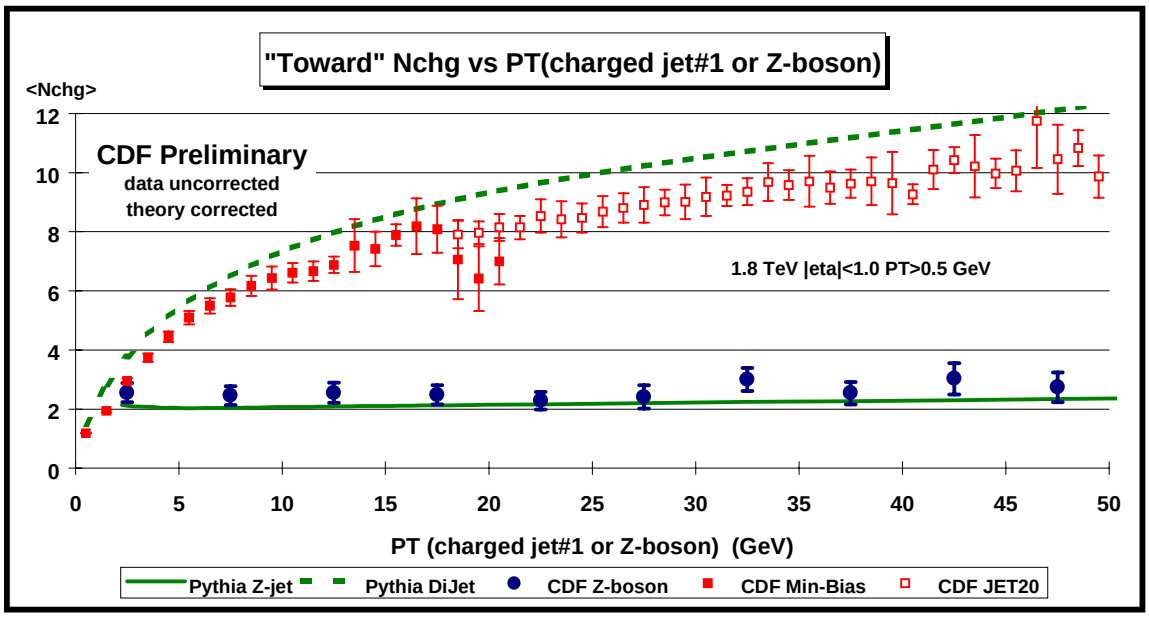

Fig. 12. Comparison of the dijet data from Fig. 5 and the Z-boson data from Fig. 7 on the average number of charged particles ($P_T > 0.5$ GeV and $|\eta| < 1$) for the "toward" region defined in Fig. 4. The plot shows the QCD Monte-Carlo predictions of PYTHIA 6.115 for dijet (dashed) and "Z-jet" (solid) production. The errors on the (*uncorrected*) data include both statistical and correlated systematic uncertainties. The theory curves are corrected for the track finding efficiency and have an error (*statistical plus systematic*) of around 5%.

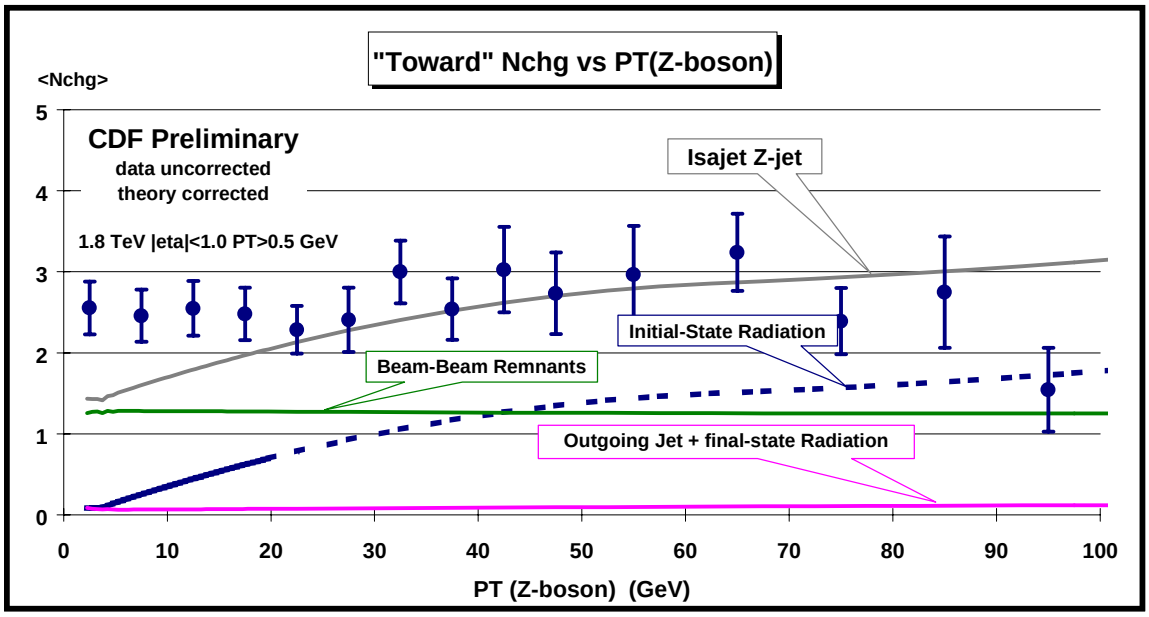

Fig. 13. Z-boson data from Fig. 7 on the average number of charged particles ($P_T > 0.5$ GeV and $|\eta| < 1$) as a function of $P_T(Z)$ for the "toward" region defined in Fig. 4 compared with the "Z-jet" QCD Monte-Carlo predictions of ISAJET 7.32. The predictions of ISAJET are divided into three categories: charged particles that arise from the break-up of the beam and target (*beam-beam remnants*), charged particles that arise from initial-state radiation, and charged particles that result from the outgoing jets plus final-state radiation (see Fig. 3). The errors on the (*uncorrected*) data include both statistical and correlated systematic uncertainties. The theory curves are corrected for the track finding efficiency and have an error (*statistical plus systematic*) of around 5%.

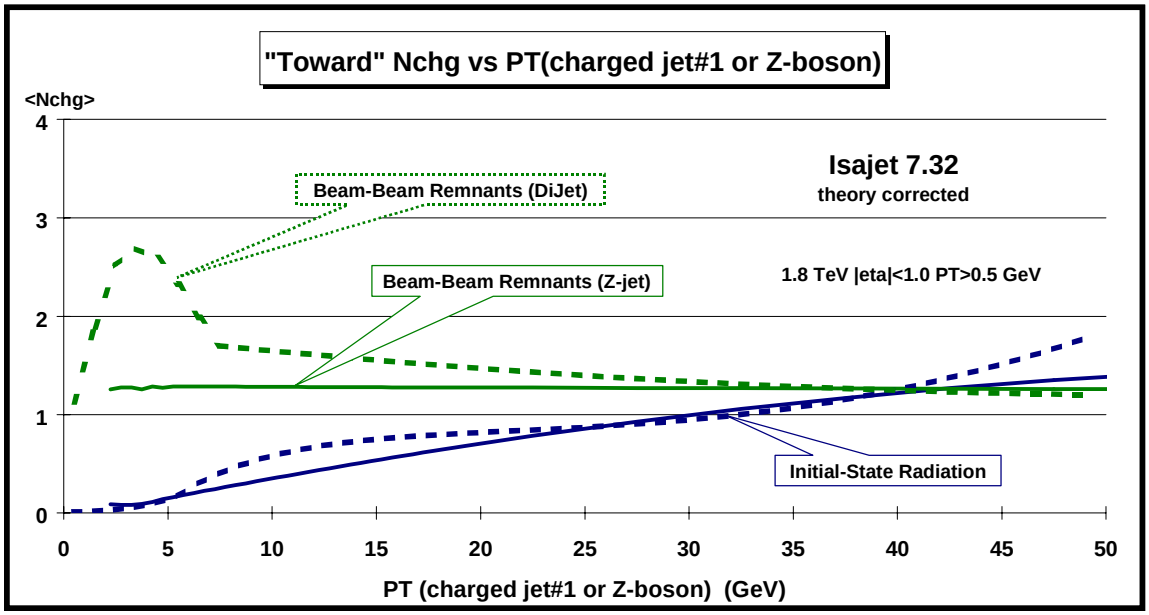

Fig. 14. Comparison of the QCD Monte-Carlo predictions of ISAJET 7.32 for the average number of charged particles ($P_T > 0.5$ GeV and $|\eta| < 1$) for the "toward" region defined in Fig. 4 for dijet (dashed) and "Z-jet" (solid) production. The plot shows the charged particles that arise from the break-up of the beam and target (*beam-beam remnants*) and the charged particles that arise from from initial-state radiation (see Fig. 1 and Fig. 3). The curves are corrected for the track finding efficiency and have an error (*statistical plus systematic*) of around 5%.

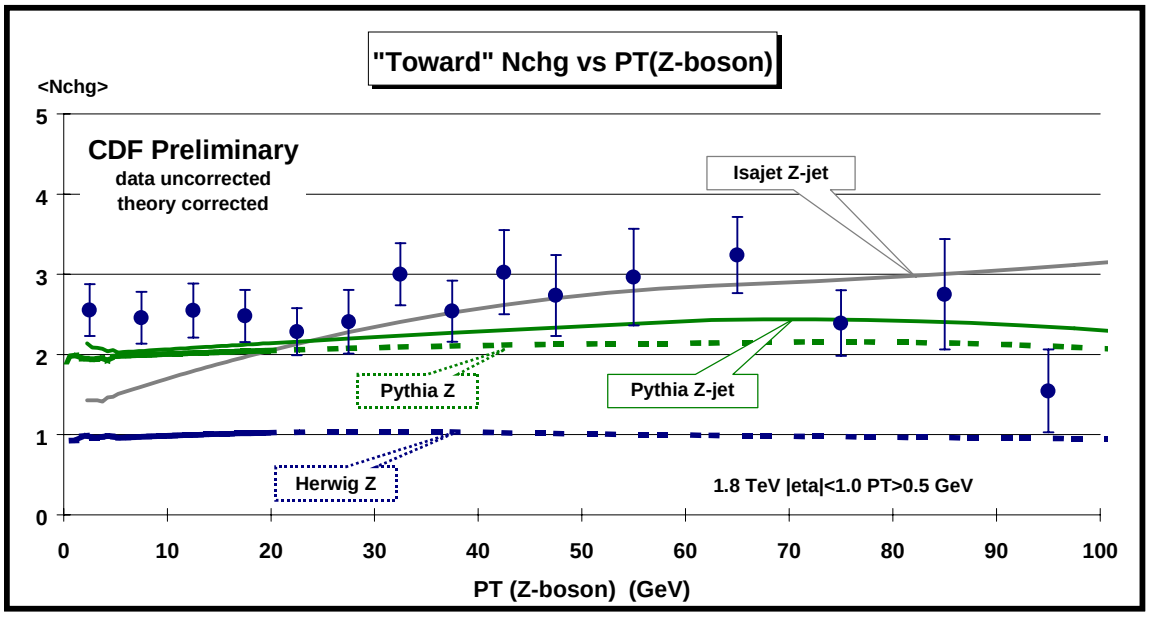

Fig. 15. Z-boson data from Fig. 7 on the average number of charged particles ($P_T > 0.5$ GeV and $|\eta| < 1$) as a function of $P_T(Z)$ for the "toward" region defined in Fig. 4 compared with the QCD Monte-Carlo predictions of HERWIG 5.9 ("Z"), ISAJET 7.32 ("Z-jet"), and PYTHIA 6.115 ("Z", "Z-jet") (see table 3). The errors on the (*uncorrected*) data include both statistical and correlated systematic uncertainties. The theory curves are corrected for the track finding efficiency and have an error (*statistical plus systematic*) of around 5%.

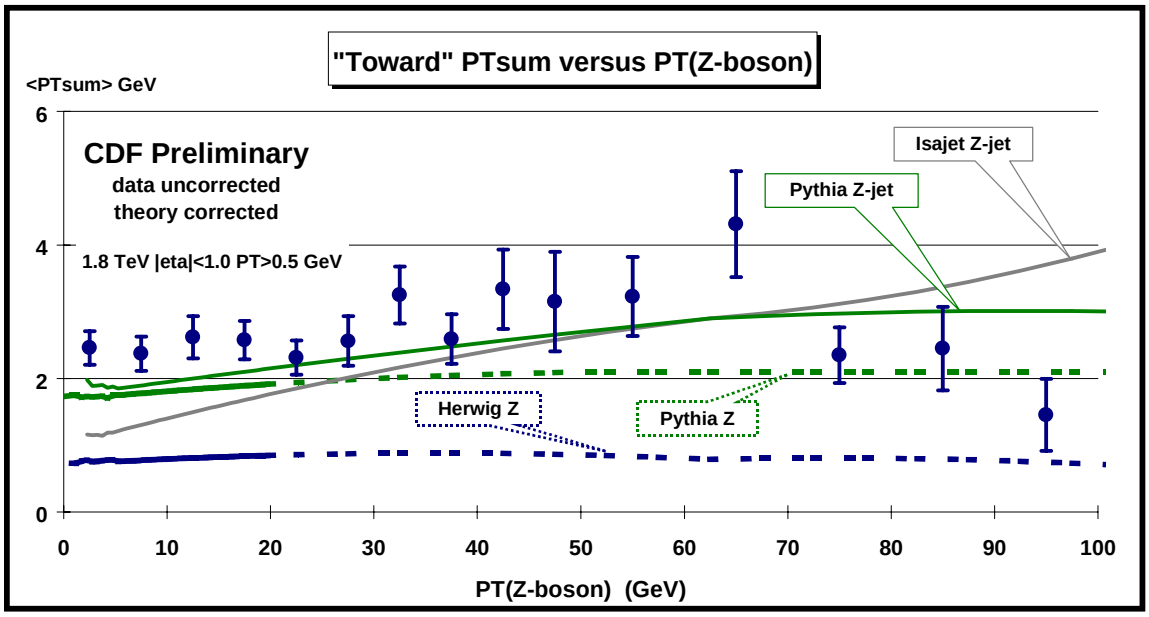

Fig. 16. Z-boson data from Fig. 8 on the average *scalar* P_T sum of charged particles ($P_T > 0.5$ GeV and $|\eta| < 1$) as a function of $P_T(Z)$ for the "toward" region defined in Fig. 4 compared with the QCD Monte-Carlo predictions of HERWIG 5.9 ("Z"), ISAJET 7.32 ("Z-jet"), and PYTHIA 6.115 ("Z", "Z-jet") (see table 3). The errors on the (*uncorrected*) data include both statistical and correlated systematic uncertainties. The theory curves are corrected for the track finding efficiency and have an error (*statistical plus systematic*) of around 5%.

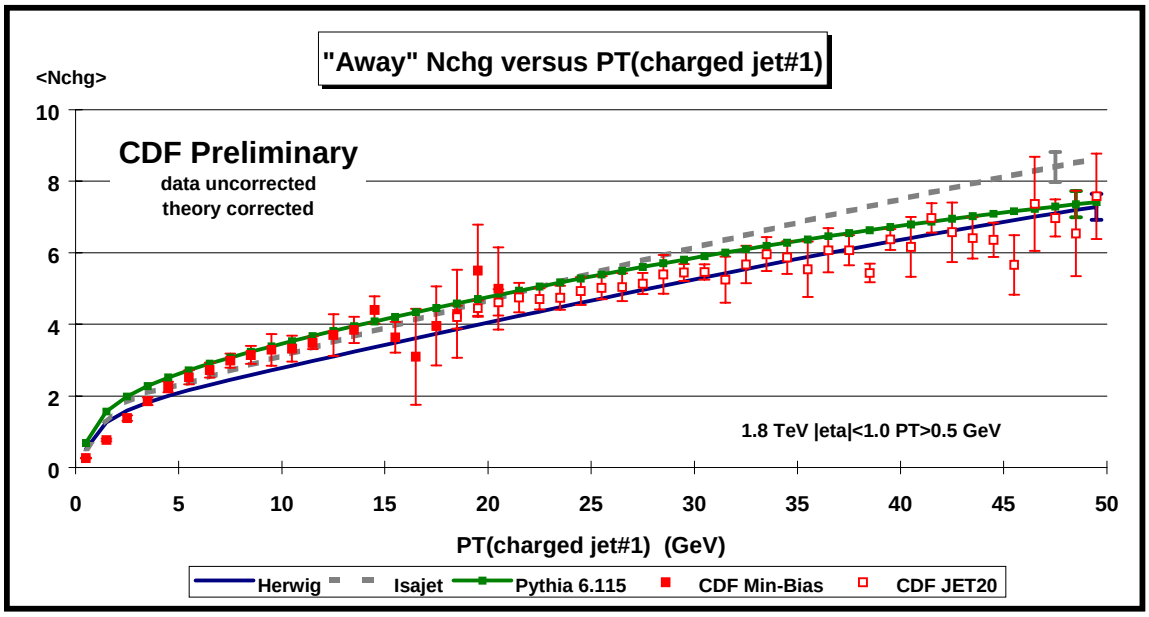

Fig. 17. Dijet data from Fig. 5 on the average number of charged particles ($P_T > 0.5$ GeV and $|\eta| < 1$) as a function of P_T(jet#1) (*leading charged jet*) for the "away" region defined in Fig. 4 compared with the QCD "hard scattering" Monte-Carlo predictions of HERWIG 5.9, ISAJET 7.32, and PYTHIA 6.115. The errors on the (*uncorrected*) data include both statistical and correlated systematic uncertainties. The theory curves are corrected for the track finding efficiency and have an error (*statistical plus systematic*) of around 5%.

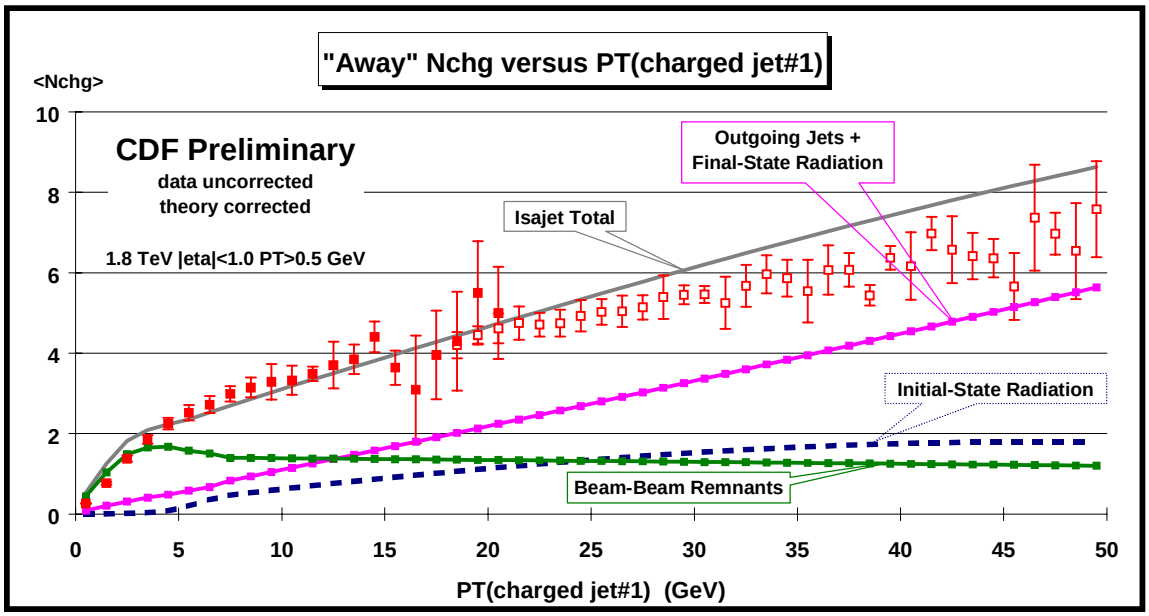

Fig. 18. Dijet data from Fig. 5 on the average number of charged particles ($P_T > 0.5$ GeV and $|\eta| < 1$) as a function of P_T(jet#1) (*leading charged jet*) for the "away" region defined in Fig. 4 compared with the QCD "hard scattering" Monte-Carlo predictions of ISAJET 7.32. The predictions of ISAJET are divided into three categories: charged particles that arise from the break-up of the beam and target (*beam-beam remnants*), charged particles that arise from initial-state radiation, and charged particles that result from the outgoing jets plus final-state radiation (see Fig. 1). The errors on the (*uncorrected*) data include both statistical and correlated systematic uncertainties. The theory curves are corrected for the track finding efficiency and have an error (*statistical plus systematic*) of around 5%.

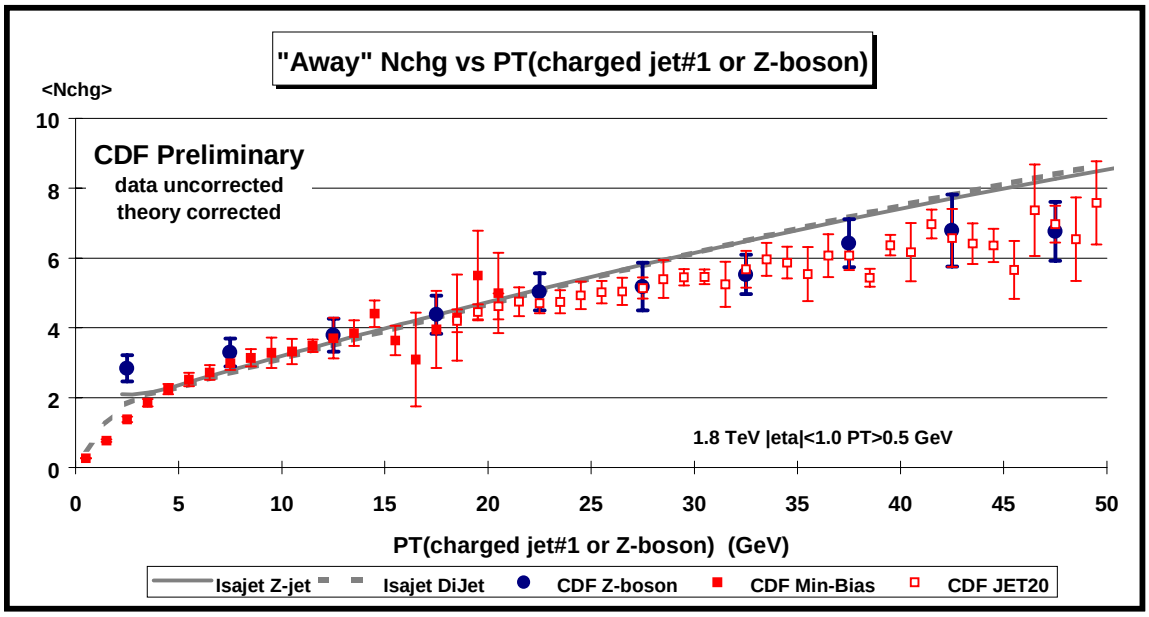

Fig. 19. Comparison of the dijet data from Fig. 5 and the Z-boson data from Fig. 7 on the average number of charged particles ($P_T > 0.5$ GeV and $|\eta| < 1$) for the "away" region defined in Fig. 4. The plot shows the QCD Monte-Carlo predictions of ISAJET 7.32 for dijet (dashed) and "Z-jet" (solid) production. The errors on the (*uncorrected*) data include both statistical and correlated systematic uncertainties. The theory curves are corrected for the track finding efficiency and have an error (*statistical plus systematic*) of around 5%.

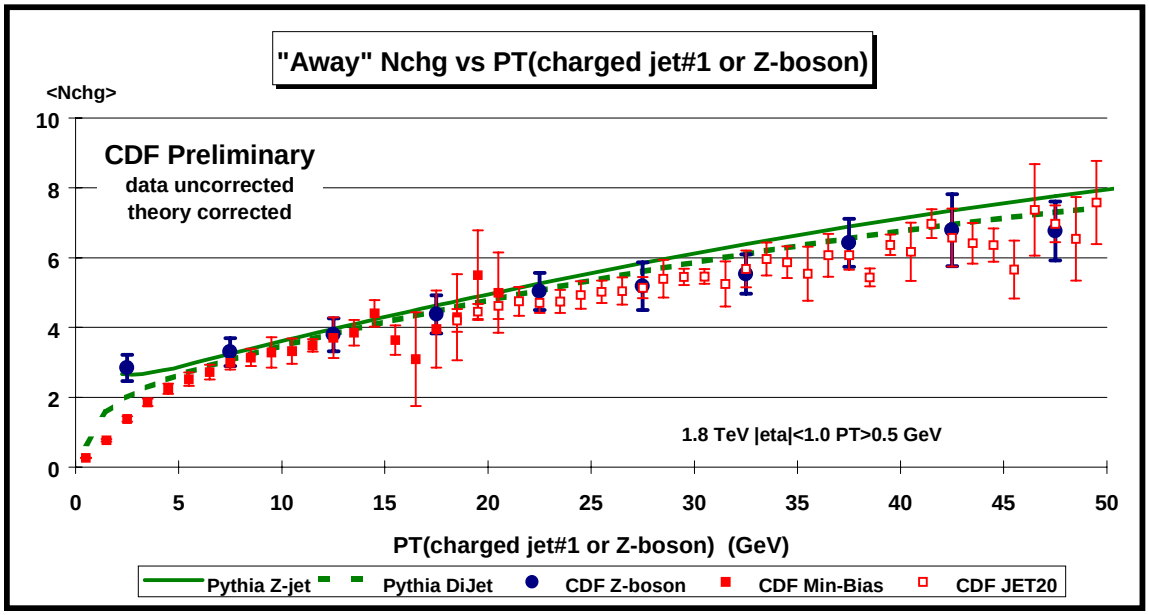

Fig. 20. Comparison of the dijet data from Fig. 5 and the Z-boson data from Fig. 7 on the average number of charged particles ($P_T > 0.5$ GeV and $|\eta| < 1$) for the "away" region defined in Fig. 4. The plot shows the QCD Monte-Carlo predictions of PYTHIA 6.115 for dijet (dashed) and "Z-jet" (solid) production. The errors on the (*uncorrected*) data include both statistical and correlated systematic uncertainties. The theory curves are corrected for the track finding efficiency and have an error (*statistical plus systematic*) of around 5%.

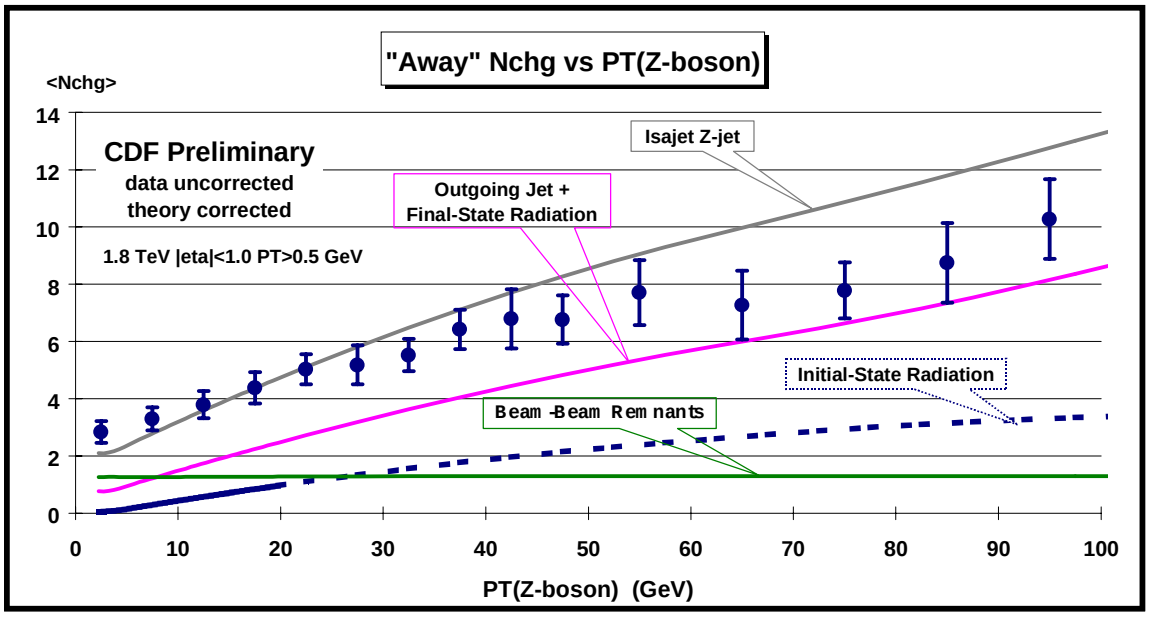

Fig. 21. Z-boson data from Fig. 7 on the average number of charged particles ($P_T > 0.5$ GeV and $|\eta| < 1$) as a function of PT(Z) for the "away" region defined in Fig. 4 compared with the "Z-jet" QCD Monte-Carlo predictions of ISAJET 7.32. The predictions of ISAJET are divided into three categories: charged particles that arise from the break-up of the beam and target (*beam-beam remnants*), charged particles that arise from initial-state radiation, and charged particles that result from the outgoing jet plus final-state radiation (see Fig. 3). The errors on the (*uncorrected*) data include both statistical and correlated systematic uncertainties. The theory curves are corrected for the track finding efficiency and have an error (*statistical plus systematic*) of around 5%.

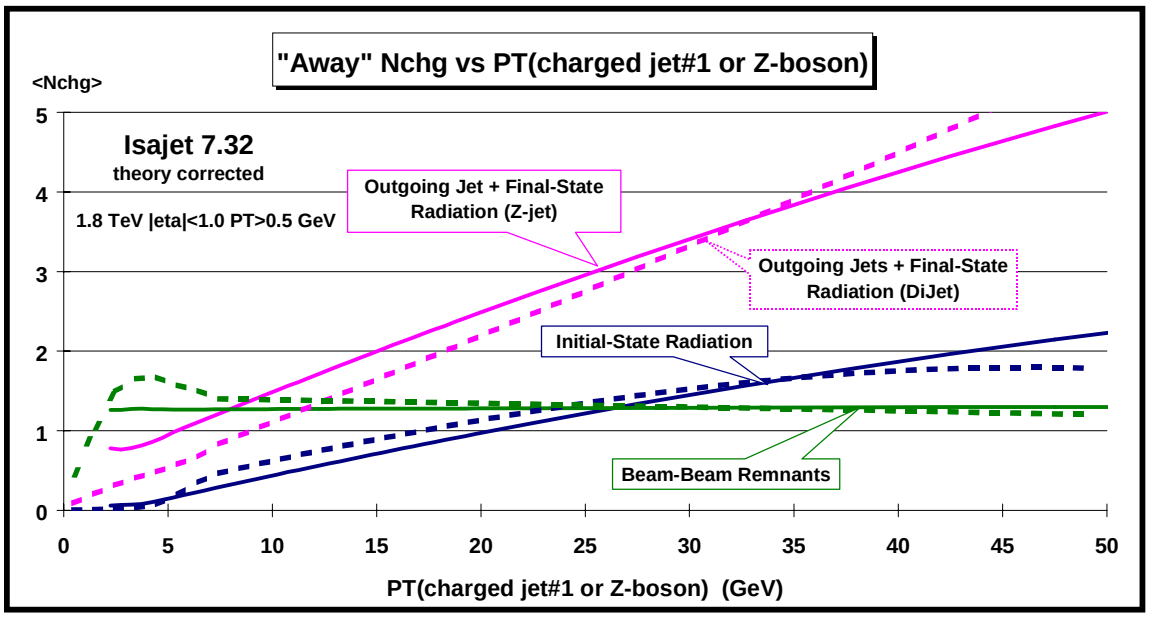

Fig. 22. Comparison of the QCD Monte-Carlo predictions of ISAJET 7.32 for the average number of charged particles ($P_T > 0.5$ GeV and $|\eta| < 1$) for the "away" region defined in Fig. 4 for dijet Fig. 18 (dashed) and "Z-jet" Fig. 21 (solid) production. The predictions of ISAJET are divided into three categories: charged particles that arise from the break-up of the beam and target (*beam-beam remnants*), charged particles that arise from initial-state radiation, and charged particles that result from the outgoing jet(s) plus final-state radiation (see Fig. 1 and Fig.3). The curves are corrected for the track finding efficiency and have an error (*statistical plus systematic*) of around 5%.

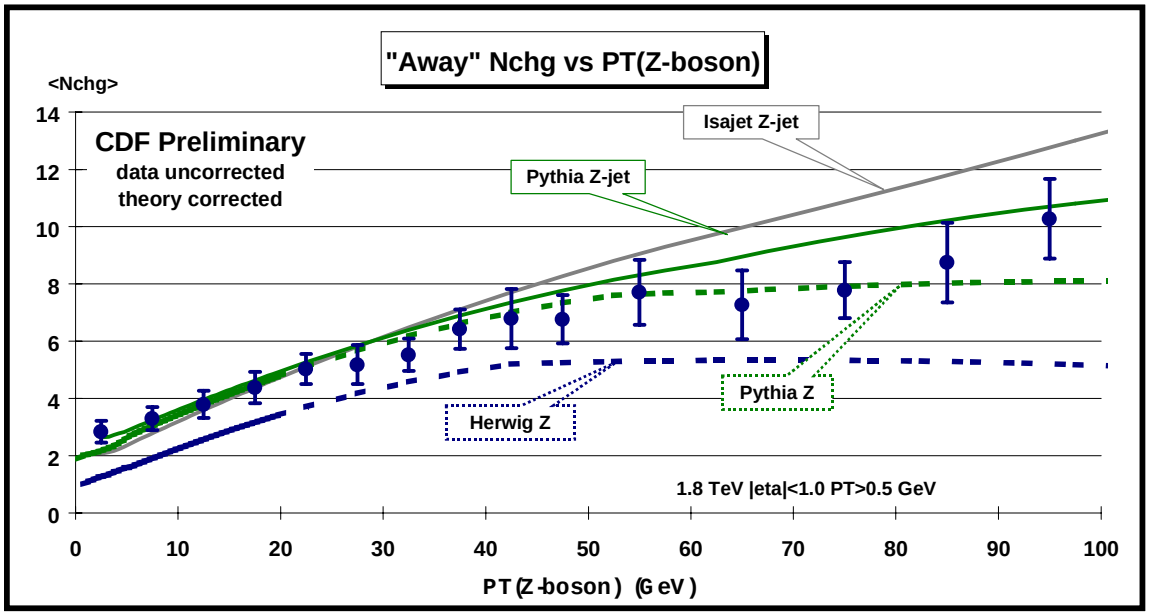

Fig. 23. Z-boson data from Fig. 7 on the average number of charged particles ($P_T > 0.5$ GeV and $|\eta| < 1$) as a function of $P_T(Z)$ for the "away" region defined in Fig. 4 compared with the QCD Monte-Carlo predictions of HERWIG 5.9 ("Z"), ISAJET 7.32 ("Z-jet"), and PYTHIA 6.115 ("Z", "Z-jet") (see table 3). The errors on the (*uncorrected*) data include both statistical and correlated systematic uncertainties. The theory curves are corrected for the track finding efficiency and have an error (*statistical plus systematic*) of around 5%.

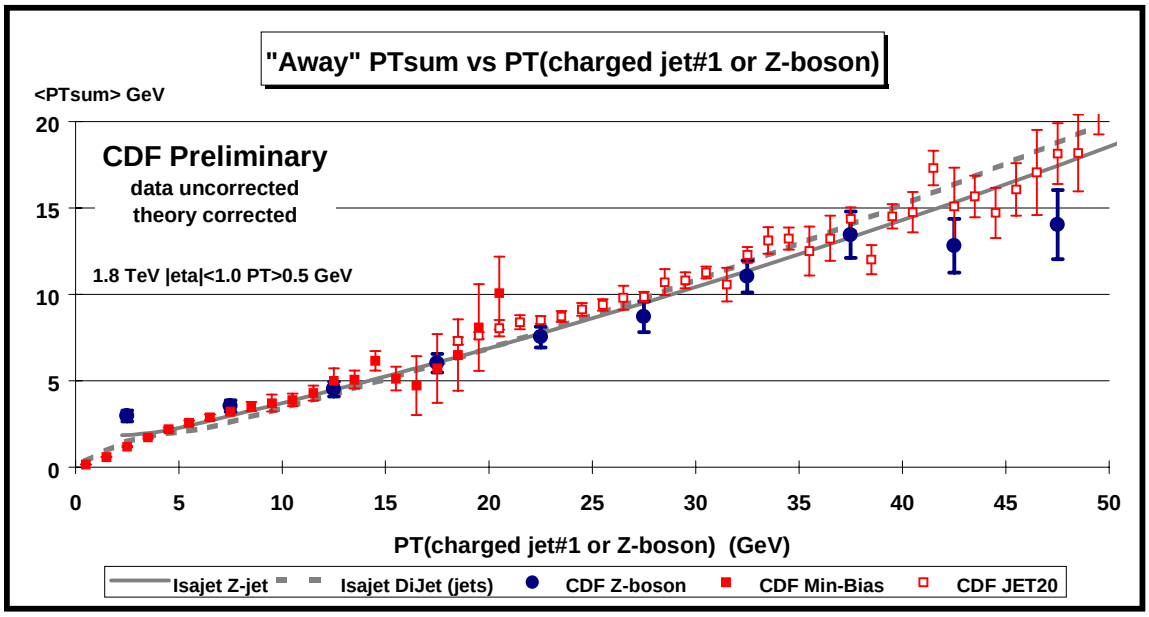

Fig. 24. Comparison of the dijet data from Fig. 6 and the Z-boson data from Fig. 8 on the average *scalar* P_T sum of charged particles ($P_T > 0.5$ GeV and $|\eta| < 1$) for the "away" region defined in Fig. 4. The plot shows the QCD Monte-Carlo predictions of ISAJET 7.32 for dijet (dashed) and "Z-jet" (solid) production. The errors on the (*uncorrected*) data include both statistical and correlated systematic uncertainties. The theory curves are corrected for the track finding efficiency and have an error (*statistical plus systematic*) of around 5%.

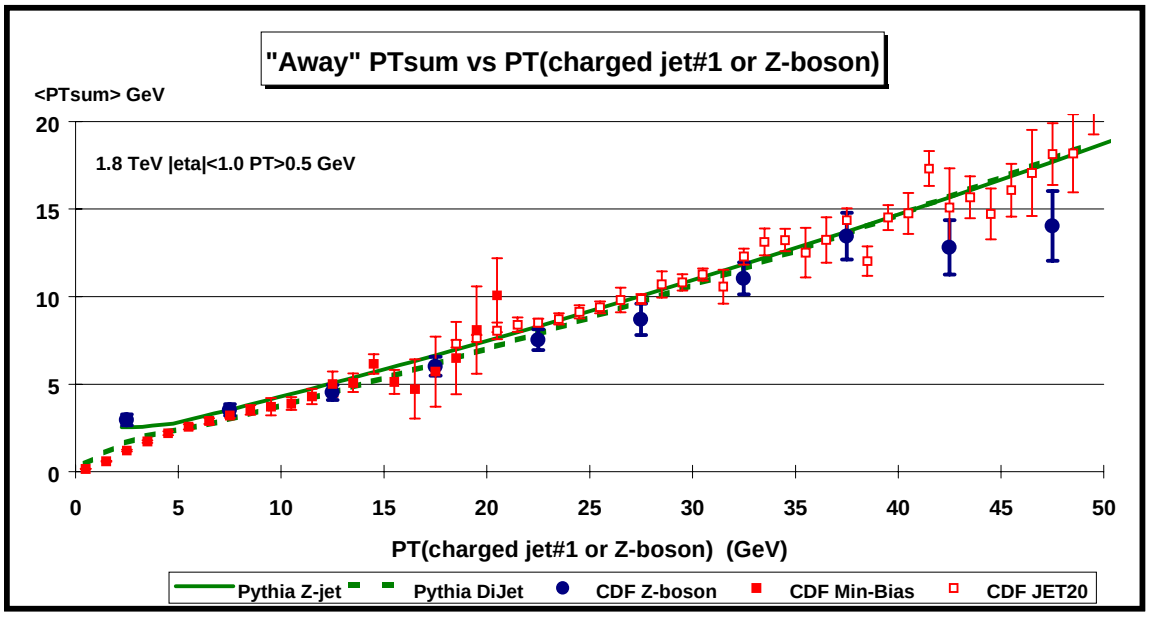

Fig. 25. Comparison of the dijet data from Fig. 6 and the Z-boson data from Fig. 8 on the average *scalar* P_T sum of charged particles ($P_T > 0.5$ GeV and $|\eta| < 1$) for the "away" region defined in Fig. 4. The plot shows the QCD Monte-Carlo predictions of PYTHIA 6.115 for dijet (dashed) and "Z-jet" (solid) production. The errors on the (*uncorrected*) data include both statistical and correlated systematic uncertainties. The theory curves are corrected for the track finding efficiency and have an error (*statistical plus systematic*) of around 5%.

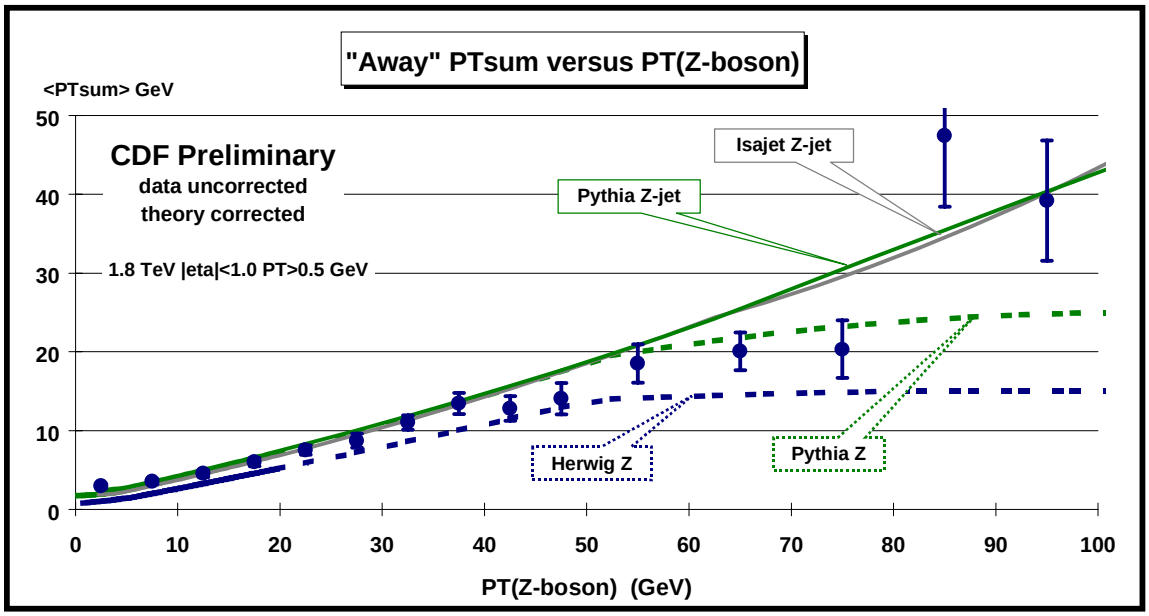

Fig. 26. Z-boson data from Fig. 8 on the average *scalar* P_T sum of charged particles ($P_T > 0.5$ GeV and $|\eta| < 1$) as a function of P_T(Z-boson) for the "away" region defined in Fig. 4 compared with the QCD Monte-Carlo predictions of HERWIG 5.9 ("Z"), ISAJET 7.32 ("Z-jet"), and PYTHIA 6.115 ("Z", "Z-jet") (see table 3). The errors on the (*uncorrected*) data include both statistical and correlated systematic uncertainties. The theory curves are corrected for the track finding efficiency and have an error (*statistical plus systematic*) of around 5%.

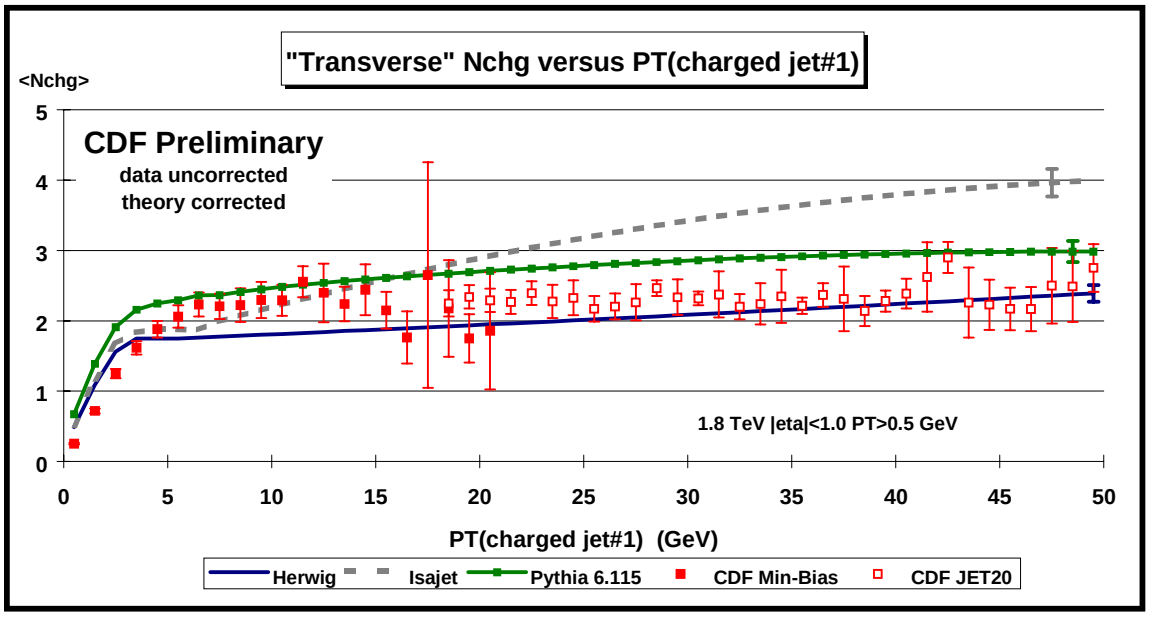

Fig. 27. Dijet data from Fig. 5 on the average number of charged particles ($P_T > 0.5$ GeV and $|\eta| < 1$) as a function of P_T(jet#1) (*leading charged jet*) for the "transverse" region defined in Fig. 4 compared with the QCD "hard scattering" Monte-Carlo predictions of HERWIG 5.9, ISAJET 7.32, and PYTHIA 6.115. The errors on the (*uncorrected*) data include both statistical and correlated systematic uncertainties. The theory curves are corrected for the track finding efficiency and have an error (*statistical plus systematic*) of around 5%.

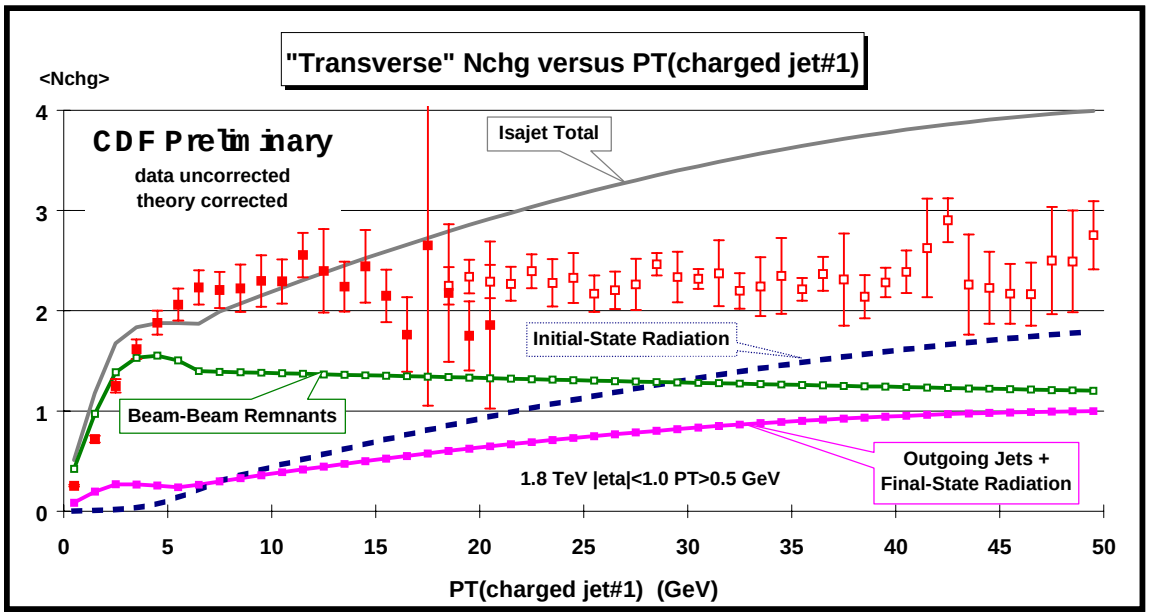

Fig. 28. Dijet data from Fig. 5 on the average number of charged particles ($P_T > 0.5$ GeV and $|\eta| < 1$) as a function of P_T(jet#1) (*leading charged jet*) for the "transverse" region defined in Fig. 4 compared with the QCD "hard scattering" Monte-Carlo predictions of ISAJET 7.32. The predictions of ISAJET are divided into three categories: charged particles that arise from the break-up of the beam and target (*beam-beam remnants*), charged particles that arise from initial-state radiation, and charged particles that result from the outgoing jets plus final-state radiation (see Fig. 1). The errors on the (*uncorrected*) data include both statistical and correlated systematic uncertainties. The theory curves are corrected for the track finding efficiency and have an error (*statistical plus systematic*) of around 5%.

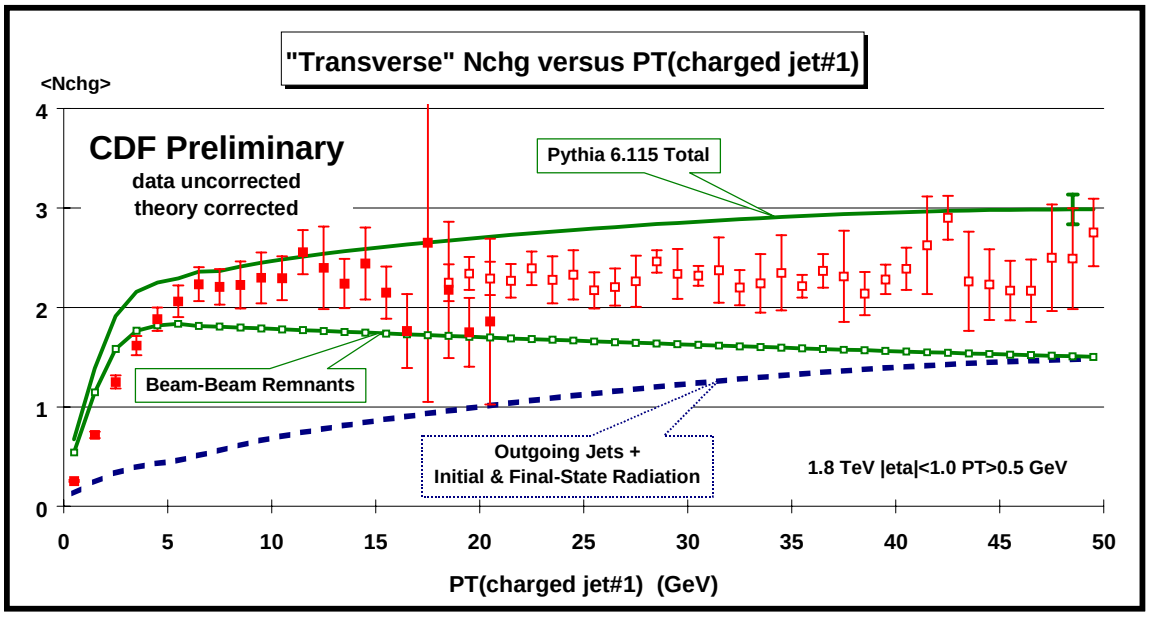

Fig. 29. Dijet data from Fig. 5 on the average number of charged particles ($P_T > 0.5$ GeV and $|\eta| < 1$) as a function of P_T(jet#1) (*leading charged jet*) for the "transverse" region defined in Fig. 4 compared with the QCD "hard scattering" Monte-Carlo predictions of PYTHIA 6.115. The predictions of PYTHIA are divided into two categories: charged particles that arise from the break-up of the beam and target (*beam-beam remnants*), and charged particles that result from the outgoing jets plus initial and final-state radiation (*hard scattering component*). For PYTHIA the beam-beam remnants include contributions from multiple parton scattering (see Fig. 2). The errors on the (*uncorrected*) data include both statistical and correlated systematic uncertainties. The theory curves are corrected for the track finding efficiency and have an error (*statistical plus systematic*) of around 5%.

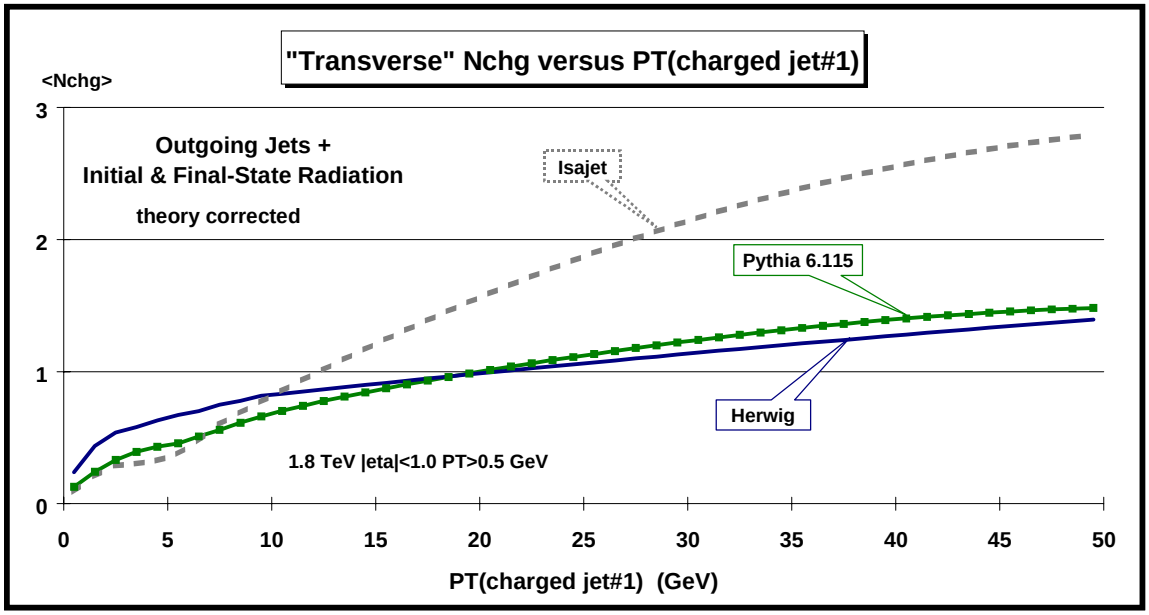

Fig. 30. QCD "hard scattering" Monte-Carlo dijet predictions from HERWIG 5.9, ISAJET 7.32, and PYTHIA 6.115 of the average number of charged particles ($P_T > 0.5$ GeV and $|\eta| < 1$) as a function of P_T(jet#1) (*leading charged jet*) for the "transverse" region defined in Fig. 4 arising from the outgoing jets plus initial and finial-state radiation (*hard scattering component*). The curves are corrected for the track finding efficiency and have an error (*statistical plus systematic*) of around 5%.

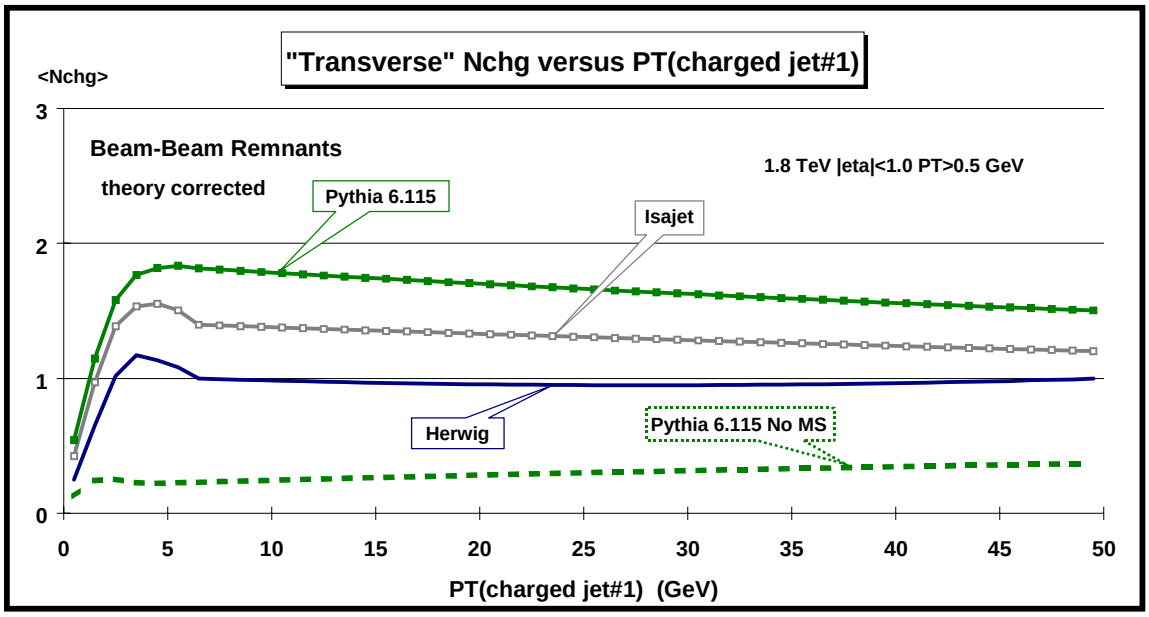

Fig. 31. QCD "hard scattering" Monte-Carlo dijet predictions from HERWIG 5.9, ISAJET 7.32, and PYTHIA 6.115 for the average number of charged particles ($P_T > 0.5$ GeV and $|\eta| < 1$) as a function of P_T(jet#1) (*leading charged jet*) for the "transverse" region defined in Fig. 4 arising from the break-up of the beam and target (*beam-beam remnants*). For PYTHIA the beam-beam remnants include contributions from multiple parton scattering (see Fig. 2). The curves are corrected for the track finding efficiency and have an error (*statistical plus systematic*) of around 5%.

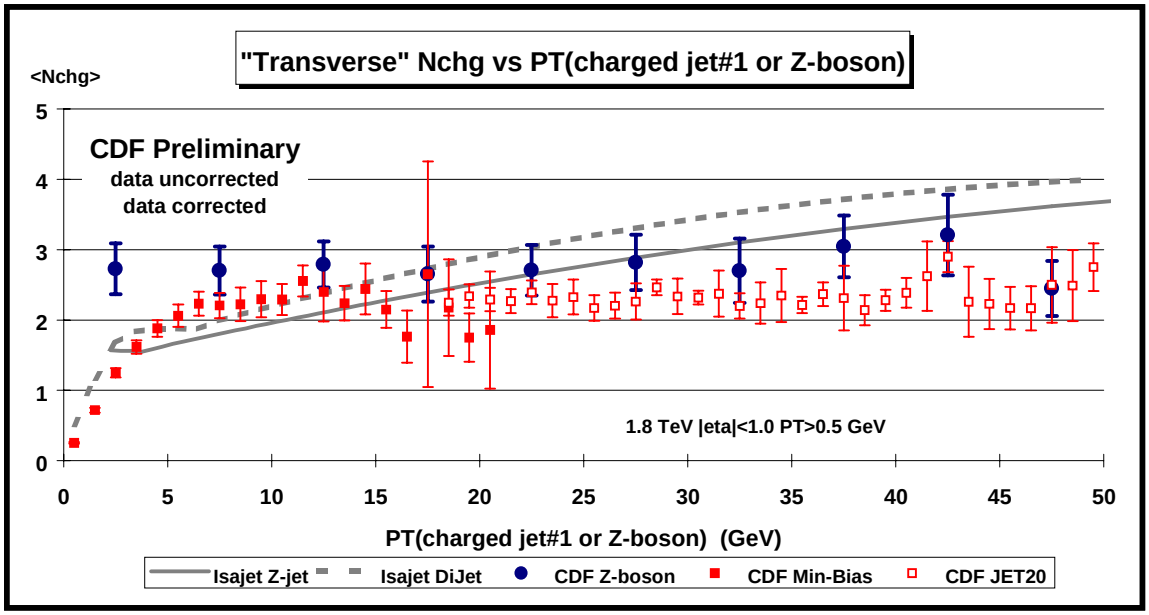

Fig. 32. Comparison of the dijet data from Fig. 5 and the Z-boson data from Fig. 7 on the average number of charged particles ($P_T > 0.5$ GeV and $|\eta| < 1$) for the "transverse" region defined in Fig. 4. The plot shows the QCD Monte-Carlo predictions of ISAJET 7.32 for dijet (dashed) and "Z-jet" (solid) production. The errors on the (*uncorrected*) data include both statistical and correlated systematic uncertainties. The theory curves are corrected for the track finding efficiency and have an error (*statistical plus systematic*) of around 5%.

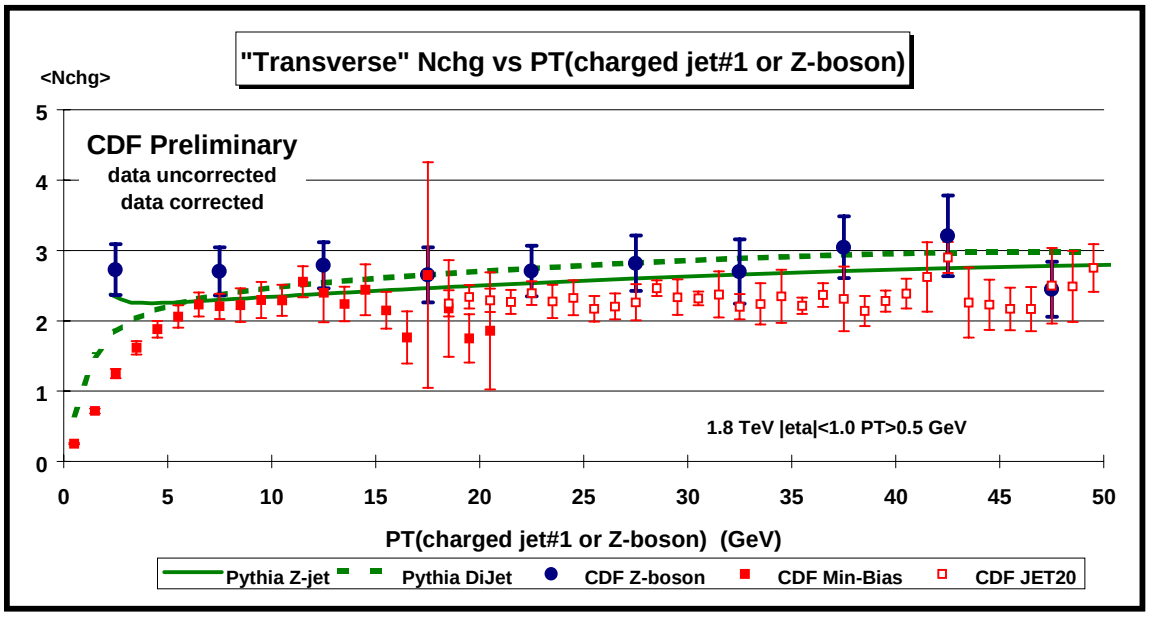

Fig. 33. Comparison of the dijet data from Fig. 5 and the Z-boson data from Fig. 7 on the average number of charged particles ($P_T > 0.5$ GeV and $|\eta| < 1$) for the "transverse" region defined in Fig. 4. The plot shows the QCD Monte-Carlo predictions of PYTHIA for dijet (dashed) and "Z-jet" (solid) production. The errors on the (*uncorrected*) data include both statistical and correlated systematic uncertainties. The theory curves are corrected for the track finding efficiency and have an error (*statistical plus systematic*) of around 5%.

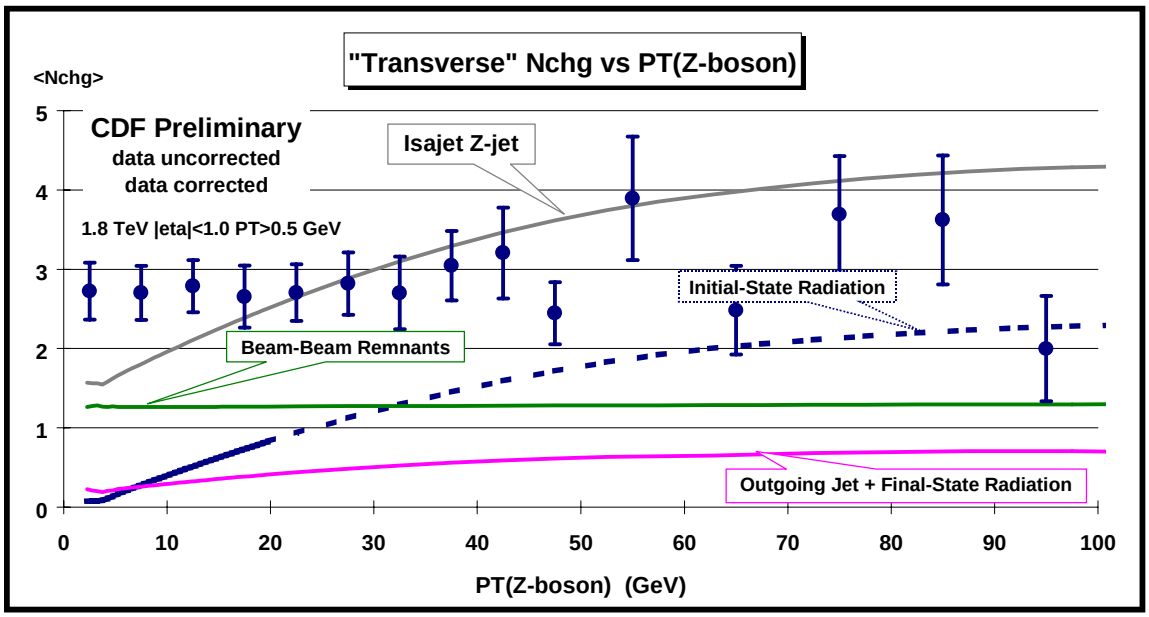

Fig. 34. Z-boson data from Fig. 7 on the average number of charged particles ($P_T > 0.5$ GeV and $|\eta| < 1$) as a function of PT(Z) for the "transverse" region defined in Fig. 4 compared with the "Z-jet" QCD Monte-Carlo predictions of ISAJET 7.32. The predictions of ISAJET are divided into three categories: charged particles that arise from the break-up of the beam and target (*beam-beam remnants*), charged particles that arise from initial-state radiation, and charged particles that result from the outgoing jet plus final-state radiation (see Fig. 2). The errors on the (*uncorrected*) data include both statistical and correlated systematic uncertainties. The theory curves are corrected for the track finding efficiency and have an error (*statistical plus systematic*) of around 5%.

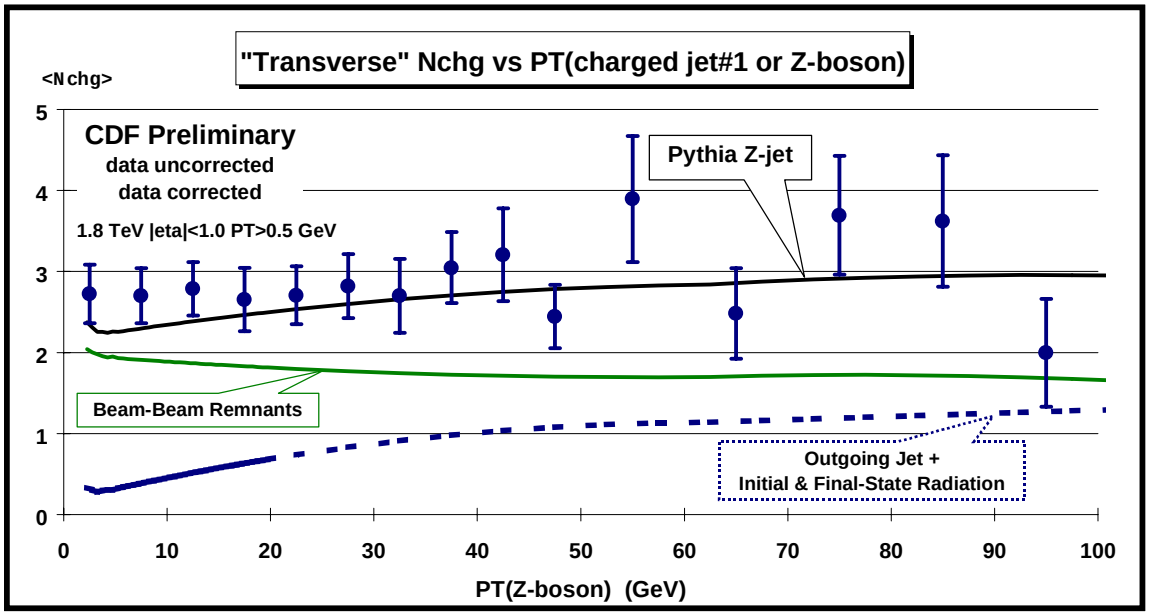

Fig. 35. Z-boson data from Fig. 7 on the average number of charged particles ($P_T > 0.5$ GeV and $|\eta| < 1$) as a function of $P_T(Z)$ for the "transverse" region defined in Fig. 4 compared with the "Z-jet" QCD Monte-Carlo predictions of PYTHIA 6.115. The predictions of PYTHIA are divided into two categories: charged particles that arise from the break-up of the beam and target (*beam-beam remnants*), and charged particles that result from the outgoing jet plus initial and final-state radiation (*hard scattering component*). For PYTHIA the beam-beam remnants include contributions from multiple parton scattering (see Fig. 2). The errors on the (*uncorrected*) data include both statistical and correlated systematic uncertainties. The theory curves are corrected for the track finding efficiency and have an error (*statistical plus systematic*) of around 5%.

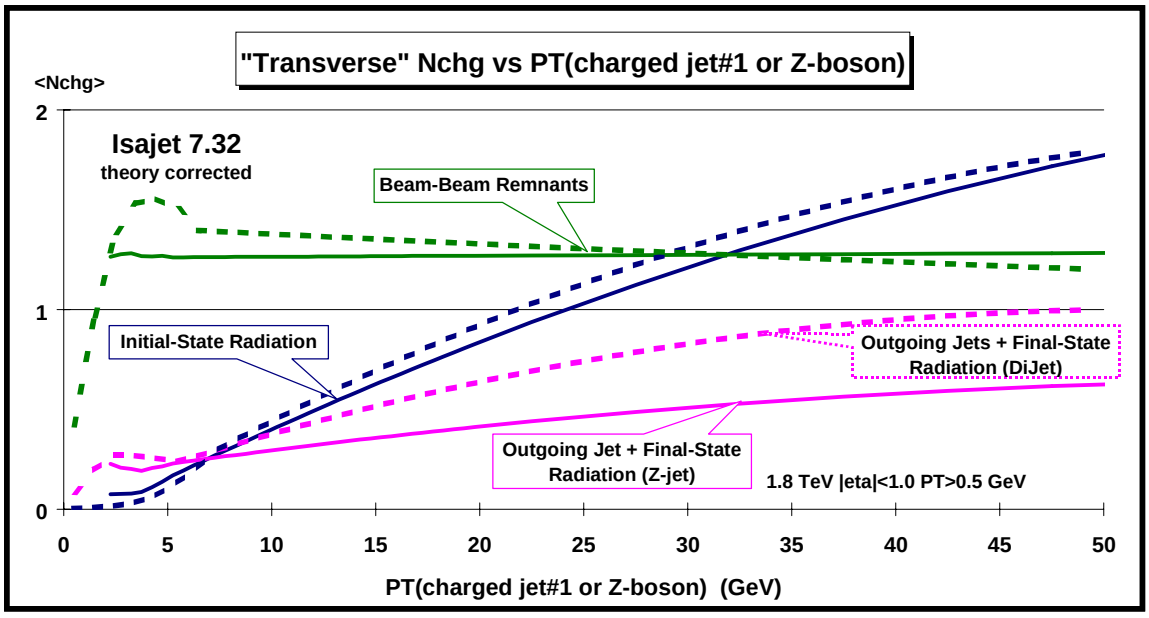

Fig. 36. Comparison of the QCD Monte-Carlo predictions of ISAJET 7.32 for the average number of charged particles ($P_T > 0.5$ GeV and $|\eta| < 1$) for the "transverse" region defined in Fig. 4 for dijet (dashed) and "Z-jet" (solid) production. The predictions of ISAJET are divided into three categories: charged particles that arise from the break-up of the beam and target (*beam-beam remnants*), charged particles that arise from initial-state radiation, and charged particles that result from the outgoing jets plus final-state radiation (see Fig. 1 and Fig. 3). The curves are corrected for the track finding efficiency and have an error (*statistical plus systematic*) of around 5%.

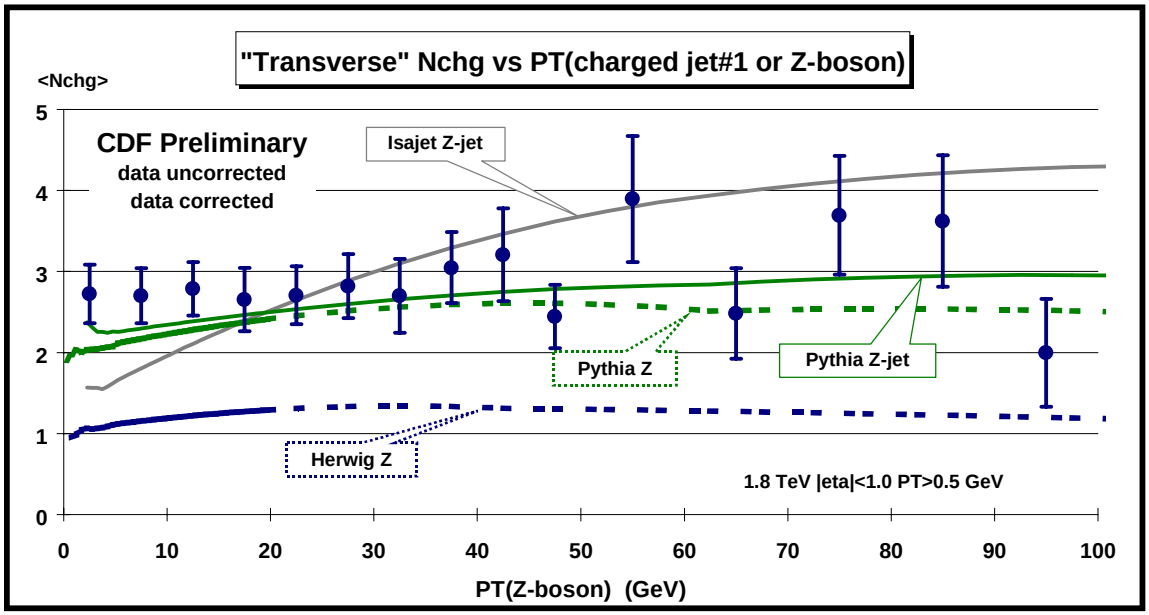

Fig. 37. Z-boson data from Fig. 7 on the average number of charged particles ($P_T > 0.5$ GeV and $|\eta| < 1$) as a function of $P_T(Z)$ for the "transverse" region defined in Fig. 4 compared with the QCD Monte-Carlo predictions of HERWIG 5.9 ("Z"), ISAJET 7.32 ("Z-jet"), and PYTHIA 6.115 ("Z", "Z-jet") (see table 3). The errors on the (*uncorrected*) data include both statistical and correlated systematic uncertainties. The theory curves are corrected for the track finding efficiency and have an error (*statistical plus systematic*) of around 5%.

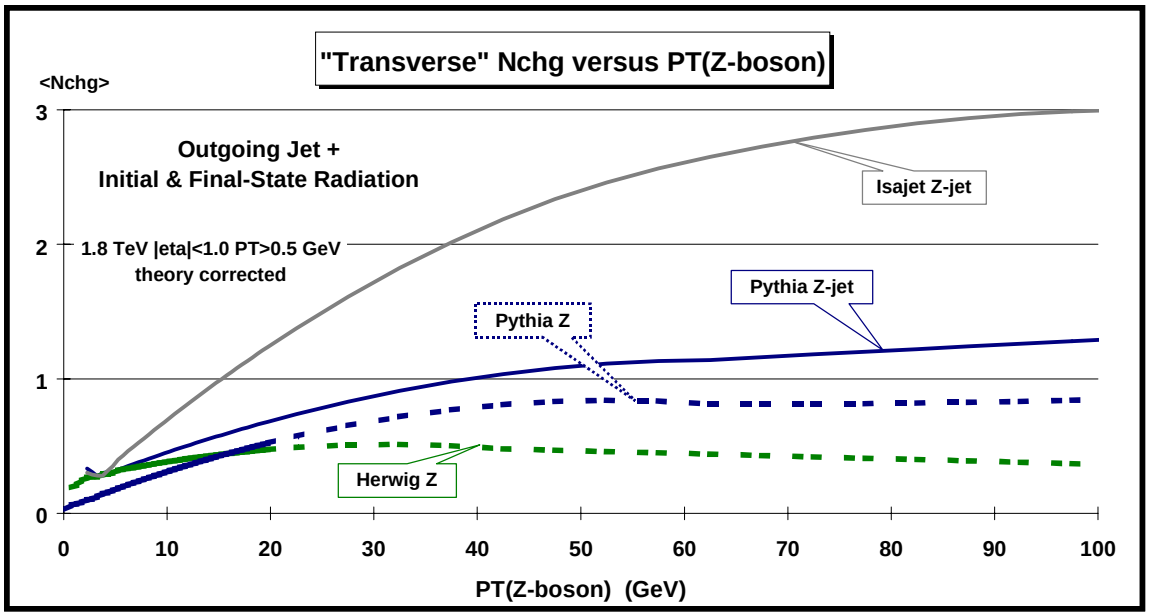

Fig. 38. QCD Monte-Carlo predictions from HERWIG 5.9 ("Z"), ISAJET 7.32 ("Z-jet"), and PYTHIA 6.115 ("Z", "Z-jet") of the average number of charged particles ($P_T > 0.5$ GeV and $|\eta| < 1$) as a function of $P_T(Z)$ for the "transverse" region defined in Fig. 4 arising from the outgoing jet plus initial & finall-state radiation (*hard scattering component*). The curves are corrected for the track finding efficiency and have an error (*statistical plus systematic*) of around 5%.

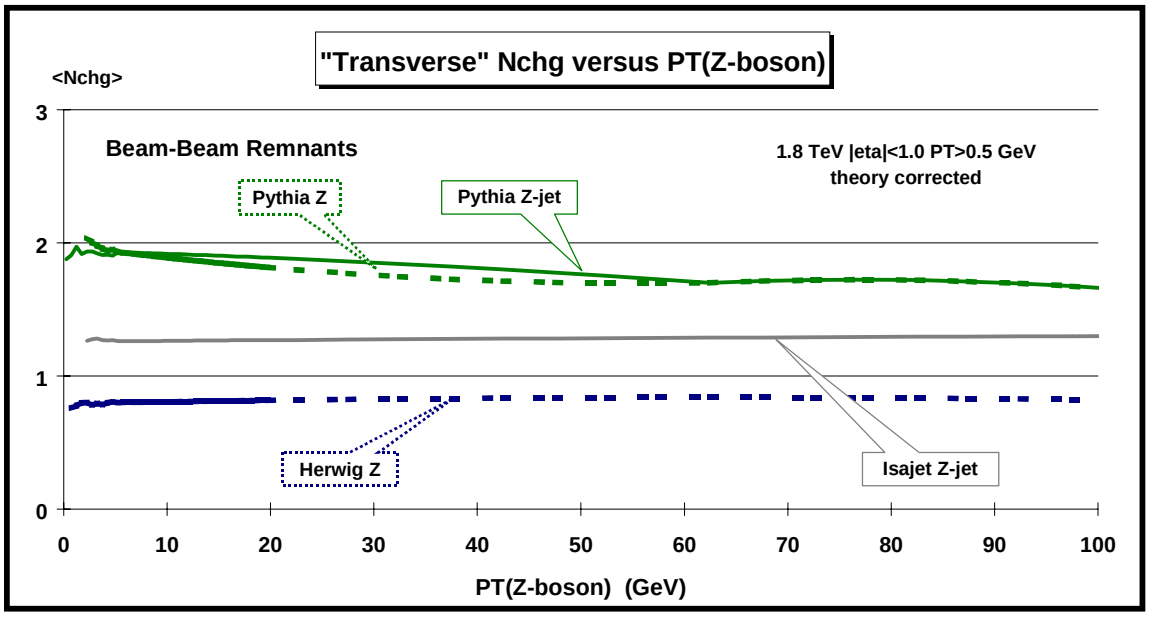

Fig. 39. QCD Monte-Carlo predictions from HERWIG 5.9 ("Z"), ISAJET 7.32 ("Z-jet"), and PYTHIA 6.115 ("Z", "Z-jet") of the average number of charged particles ($P_T > 0.5$ GeV and $|\eta| < 1$) as a function of $P_T(Z)$ for the "transverse" region defined in Fig. 4 arising from the break-up of the beam and target (*beam-beam remnants*). For PYTHIA the beam-beam remnants include contributions from multiple parton scattering (see Fig. 2). The curves are corrected for the track finding efficiency and have an error (*statistical plus systematic*) of around 5%.

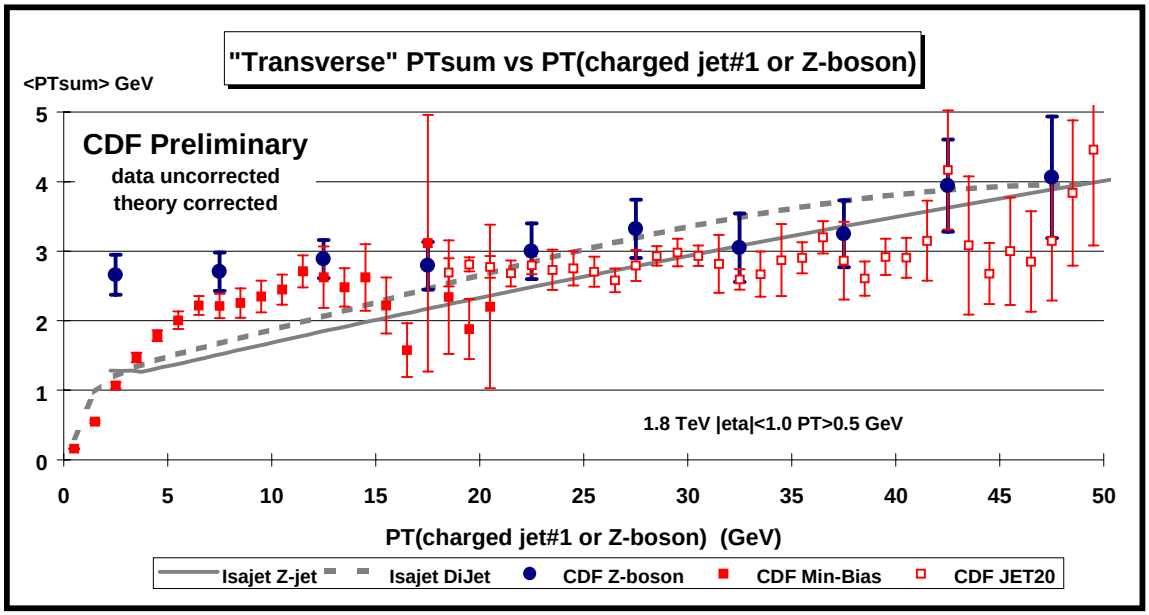

Fig. 40. Comparison of the dijet data from Fig. 6 and the Z-boson data from Fig. 8 on the average *scalar* PT sum of charged particles ($P_T > 0.5$ GeV and $|\eta| < 1$) for the "transverse" region defined in Fig. 4. The plot shows the QCD Monte-Carlo predictions of ISAJET for dijet (dashed) and "Z-jet" (solid) production. The errors on the (*uncorrected*) data include both statistical and correlated systematic uncertainties. The theory curves are corrected for the track finding efficiency and have an error (*statistical plus systematic*) of around 5%.

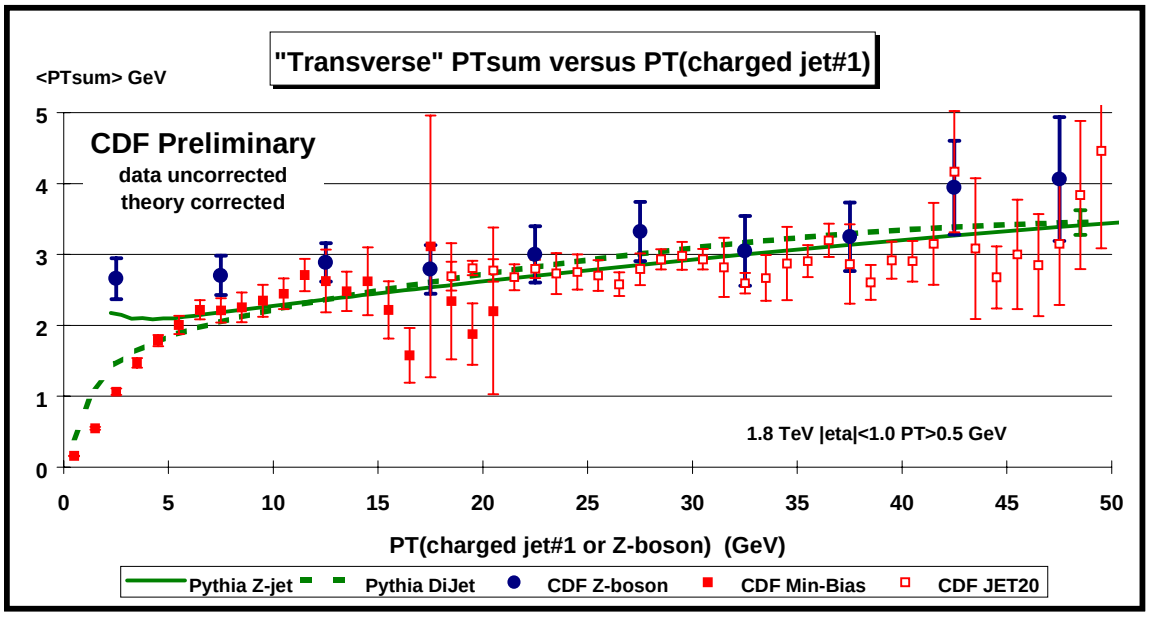

Fig. 41. Comparison of the dijet data from Fig. 6 and the Z-boson data from Fig. 8 on the average *scalar* PT sum of charged particles ($P_T > 0.5$ GeV and $|\eta| < 1$) for the "transverse" region defined in Fig. 4. The plot shows the QCD Monte-Carlo predictions of HERWIG for dijet (dashed) and "Z-jet" (solid) production. The errors on the (*uncorrected*) data include both statistical and correlated systematic uncertainties. The theory curves are corrected for the track finding efficiency and have an error (*statistical plus systematic*) of around 5%.

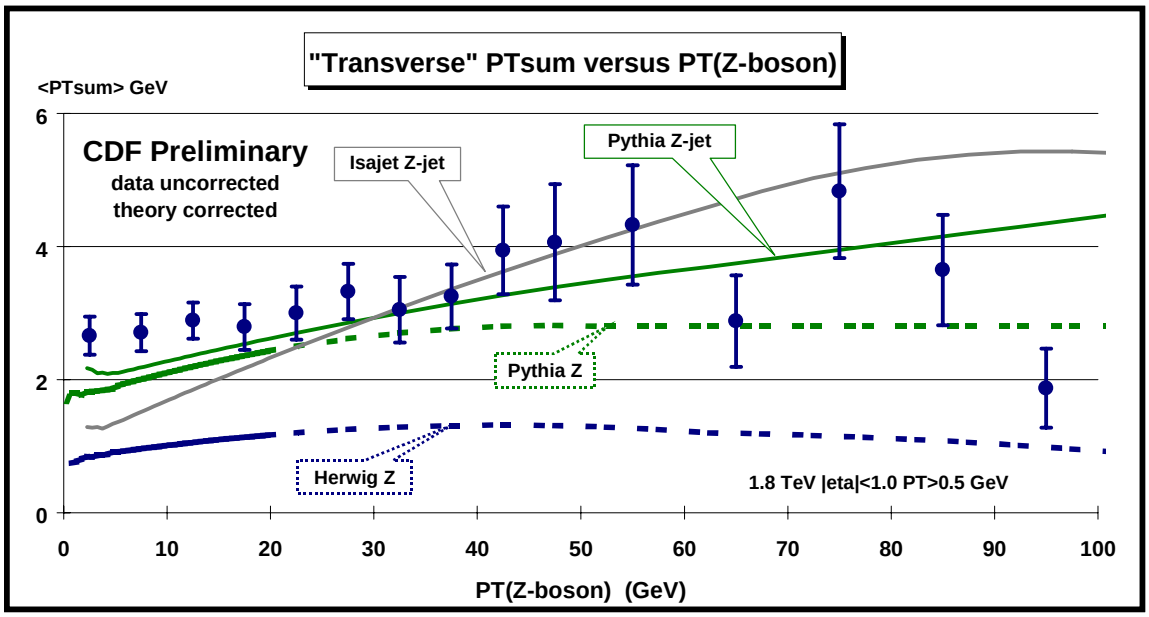

Fig. 42. Z-boson data from Fig. 8 on the average *scalar* P_T sum of charged particles ($P_T > 0.5$ GeV and $|\eta| < 1$) as a function of $P_T(Z)$ for the "transverse" region defined in Fig. 4 compared with the QCD Monte-Carlo predictions of HERWIG 5.9 ("Z"), ISAJET 7.32 ("Z-jet"), and PYTHIA 6.115 ("Z", "Z-jet") (see table 3). The errors on the (*uncorrected*) data include both statistical and correlated systematic uncertainties. The theory curves are corrected for the track finding efficiency and have an error (*statistical plus systematic*) of around 5%.